Article

SOURCE
DATA

TRANSPARENT
PROCESS

EMBO
reports

The p38-interacting protein p38IP suppresses TCR and LPS signaling by targeting TAK1

Xu-Dong Wang[1],[†] , Chen-Si Zhao[1],[†] , Qi-Long Wang[1], Qi Zeng[1], Xing-Zhi Feng[1], Lianbo Li[2], Zhi-Long Chen[1] , Yu Gong[1], Jiahuai Han[3] & Yingqiu Li[1],*

Abstract

Negative regulation of immunoreceptor signaling is required for preventing hyperimmune activation and maintaining immune homeostasis. The roles of p38IP in immunoreceptor signaling remain unclear. Here, we show that p38IP suppresses T-cell receptor (TCR)/LPS-activated NF-κB and p38 by targeting TAK1 kinase and that p38IP protein levels are downregulated in human PBMCs from rheumatoid arthritis (RA) patients, inversely correlating with the enhanced activity of NF-κB and p38. Mechanistically, p38IP interacts with TAK1 to disassemble the TAK1-TAB (TAK1-binding protein) complex. p38IP overexpression decreases TCR-induced binding of K63-linked polyubiquitin (polyUb) chains to TAK1 but increases that to TAB2, and p38IP knockdown shows the opposite effects, indicating unanchored K63-linked polyUb chain transfer from TAB2 to TAK1. p38IP dynamically interacts with TAK1 upon stimulation, because of the polyUb chain transfer and the higher binding affinity of TAK1 and p38IP for polyUb-bound TAB2 and TAK1, respectively. Moreover, p38IP scaffolds the deubiquitinase USP4 to deubiquitinate TAK1 once TAK1 is activated. These findings reveal a novel role and the mechanisms of p38IP in controlling TCR/LPS signaling and suggest that p38IP might participate in RA pathogenesis.

Introduction

p38-interacting protein (p38IP) was first identified as a p38 binding partner in a yeast two-hybrid analysis (NCBI accession number AF093250). A genetic study revealed that p38IP is required for p38 activation and E-cadherin downregulation during mouse gastrulation [1]. By mass spectrometry, p38IP was found to be a mammalian protein homologous to yeast ySpt20, which is a specific subunit of the Spt-Ada-Gcn5 acetyltransferase (SAGA) coactivator complex but not the human ADA2A-containing acetyltransferase complex (ATAC), an evolutionarily divergent complex from p38IP-SAGA, and was found to be required for the assembly and integrity of the SAGA acetyltransferase complex [2,3]. Additionally, p38IP participates in the regulation of endoplasmic reticulum stress by binding to the promoter of endoplasmic reticulum stress-induced genes [3], and it mediates starvation-induced autophagy through the regulation of mammalian Atg9 trafficking [4]. We have shown that p38IP regulates G_2/M progression by stabilizing GCN5 [5] and controls monocyte/macrophage differentiation in the manner of a novel miR-200b-3p/p38IP pair [6]. Taken together, these discoveries depict a multifunctional characteristic of p38IP. However, how p38IP regulates p38 is unknown, and the effect of p38IP on p38 activity is still under debate. It is also not known whether p38IP participates in immune receptor-mediated signaling.

p38 MAPK and NF-κB are two crucial regulators in many physiological processes, including inflammation, innate and adaptive immunity, cell proliferation, and cell survival [7,8]. In most contexts, TGFβ-activated kinase 1 (TAK1) is the essential kinase in immune receptor-mediated activation of p38 MAPK and NF-κB [9–11]. TAK1 is usually constitutively associated with the TAK1 binding proteins TAB1 and TAB2 or TAB3, forming the heterotrimeric complexes TAK1-TAB1-TAB2 or TAK1-TAB1-TAB3 in cells [12–15]. Despite the stimulus specificity of the upstream regulators of TAK1, the formation of the TAK1-TAB complex and TAB-scaffolded linkage of polyUb chains to TAK1 are essential for TAK1 activation. TAB1 constitutively binds to the kinase domain of TAK1 and induces autophosphorylation of TAK1 at the activation loop [12,16]. Unlike TAB1, TAB2 and its homologue TAB3 cannot activate TAK1 directly [13,14]. Both TAB2 and TAB3 possess coiled-coil domains at the C-terminus that mediate their association with the last C-terminal 100 residues of TAK1 [13,15,17]; TAB2 and TAB3 also bind to K63-linked polyUb chains through a conserved Npl4 zinc finger (NZF) domain in their C-terminal ends [18,19]. By binding to both TAK1 and polyUb chains, TAB2/3 bring TAK1 in proximity to K63-linked polyUb chains [20–22]. These polyUb chains are synthesized

by the E3 ubiquitin ligase TRAF6, particularly in Toll-like receptor (TLR), TGF-β receptor, and B-cell receptor BCR/TCR signaling; by TRAF6/Pellino E3 ligases in IL-1R signaling; or by TRAF2/5 in tumor necrosis factor receptor 1 (TNFR1) signaling and in turn activate TAK1 [20–24]. The K63-linked polyUb chains that activate TAK1 could be unanchored or conjugated to TAK1 [21,25,26]. However, whether there is an intrinsic negative counterpart of TABs in the regulation of TAK1 is unknown.

Both adaptive and innate immunoreceptor signaling are tightly regulated at multiple levels by a series of negative regulators. Loss of negative regulators can cause hyperactivation of immune cells and lead to autoimmune and inflammatory diseases [27,28]. Rheumatoid arthritis (RA) is a chronic inflammatory autoimmune disease characterized by the aberrant activation of the innate and adaptive immune systems, which is caused by both genetic and environmental factors [29,30]. In particular, hyperactivation of $CD4^+$ T cells contributes to the pathogenesis of RA [30,31]. Identifying novel negative regulators of immunoreceptor signaling will provide attractive targets for therapeutic intervention in autoimmune and inflammatory diseases and cancer because inhibitors of negative regulators might enhance antitumor immunity.

In this study, we revealed that p38IP is an intrinsic negative regulator of TAK1 activation through a dual mechanism: disassembling the TAK1-TAB complex constitutively by binding to TAK1 via its TAK1-binding (T1B) domain and specifically delivering USP4 via its USP4-binding (U4B) domain to activated TAK1 to deubiquitinate it. We observed that unanchored K63-linked polyUb chains may be relayed *in vivo* as batons from TAB2 to TAK1, which is inhibited by p38IP, and further confirmed it by *in vitro* polyUb chain binding analysis. We further demonstrated both *in vivo* and *in vitro* that p38 dynamically interacts with TAK1. This dynamic is caused by the degrees of unanchored polyUb binding to TAB2 and TAK1 and the transfer of unanchored polyUb chains from TAB2 to TAK1. These findings establish that p38IP is a negative regulator of TCR/LPS signaling by acting as a negative counterpart of TABs and a specific adaptor for USP4, indicate a dynamic regulatory mechanism of TAK1, and suggest a transfer model for unanchored polyUb chains.

Results

p38IP inhibits TCR- and LPS-induced cytokine production

Our immunoblotting analysis showed that the p38IP protein is expressed in the majority of tissues, including immune-related tissues and cells such as skin, spleen, lymph nodes, thymus, lung, and peripheral blood mononuclear cells (PBMCs), but not the brain (Fig EV1A). In addition, p38 MAPK is an important kinase in inflammatory and immune responses [32], and thus, we reasoned that p38IP might have important roles in immune regulation. To determine whether p38IP is involved in the TCR signaling pathway, we first generated an sh-NC Jurkat T-cell line stably expressing a scrambled negative control small hairpin RNA (shRNA) and an sh-p38IP Jurkat T-cell line stably expressing an shRNA designed to specifically target human p38IP mRNA (Fig EV1B; Appendix Table S1). Then, using high-throughput RNA-sequencing (RNA-seq) analysis, we compared the global gene expression patterns between sh-NC cells and sh-p38IP cells after stimulation

with anti-CD3 and anti-CD28 antibodies. As a result, 205 differentially expressed genes (DEGs) were selected using the threshold of fold change > 2 in expression between the two treated groups ($P < 0.05$) and were subjected to Kyoto Encyclopedia of Genes and Genomes (KEGG), Gene Ontology (GO), and REACTOME Pathways enrichment analyses (Fig 1A–C). The KEGG pathway analysis identified 39 significantly enriched ($P < 0.05$) pathways associated with p38IP knockdown, of which the top pathways were cytokine–cytokine receptor interactions and NF-κB signaling (Fig 1A). In the GO annotation analysis, 30 biological process terms were significantly enriched in sh-p38IP cells and were mainly related to cytokine and chemokine activity and regulation (Fig 1B). REACTOME Pathways, another pathway analysis program, showed that p38IP was preferably involved in cytokine and NF-κB pathways, which was consistent with the results from the KEGG and GO analyses (Fig 1B). In p38IP knockdown cells, representative NF-κB target genes selected from the DEGs were found to be significantly upregulated, whereas the NF-κB-suppressed gene RUNX2 was downregulated (Fig 1D), and the p38-dependent DEGs were also significantly upregulated (Fig EV1C). These RNA-seq data showed that p38IP knockdown induced perturbations in the expression of cytokine- and chemokine-related genes, especially the expression of NF-κB target genes, suggesting a negative regulatory role of p38IP in TCR-induced NF-κB signaling.

To verify our RNA-seq results, we further detected TCR-induced NF-κB and p38-related cytokines at the protein level in cells with p38IP knockdown or overexpression. Intracellular cytokine staining combined with flow cytometry analysis showed that after crosslinking TCR and the coreceptor CD28 with antibodies against CD3 and CD28, the frequency of TNF-α- and IL-2-positive cells was much higher in the sh-p38IP cell line than in the sh-NC cell line (Fig 1E). To address the regulatory role of p38IP in primary cells, we isolated primary human PBMCs (50–80% T cells and 10–20% monocytes) from healthy donors and transfected them with a short interfering RNA designed to specifically target the same region in p38IP mRNA (si-p38IP) as sh-p38IP and with a scrambled siRNA (si-NC) (Fig EV1D; Appendix Table S1). ELISA analysis showed that knockdown of p38IP in human PBMCs markedly enhanced the production of IL-2 and IL-6 after CD3/CD28 stimulation (Fig 1F). Jurkat TAg T cells (a derivative of the human leukemic T-cell line Jurkat E6.1 deficient in CD28 expression and stably expressing the SV40 large T antigen, which can promote the replication of expression vectors of SV40 origin) were electroporated with a YFP-p38IP or YFP vector, and stimulated with the PKC activator phorbol 12-myristate 13-acetate (PMA) plus the Ca^{2+} ionophore ionomycin (mimicking TCR signaling by directly activating the second messengers DAG and Ca^{2+}). Exogenous expression of p38IP significantly reduced PMA/ionomycin-induced production of TNF-α mRNA (Fig EV1E) and the production of TNF-α and IL-2 proteins (Fig EV1F).

Next, we determined whether p38IP was involved in the LPS signaling pathway by knocking down endogenous p38IP expression in RAW264.7 cells (a murine *macrophage* cell line) with two short interfering RNAs (siRNAs) designed specifically to target different regions of murine p38IP mRNA (si-mp38IP-1 and si-mp38IP-2; Appendix Table S1). Immunoblotting analysis revealed that both si-mp38IP-1 and si-mp38IP-2 efficiently knocked down p38IP protein expression relative to the control scrambled siRNA (si-NC) (Fig EV1G). Real-time PCR analysis revealed that knockdown of
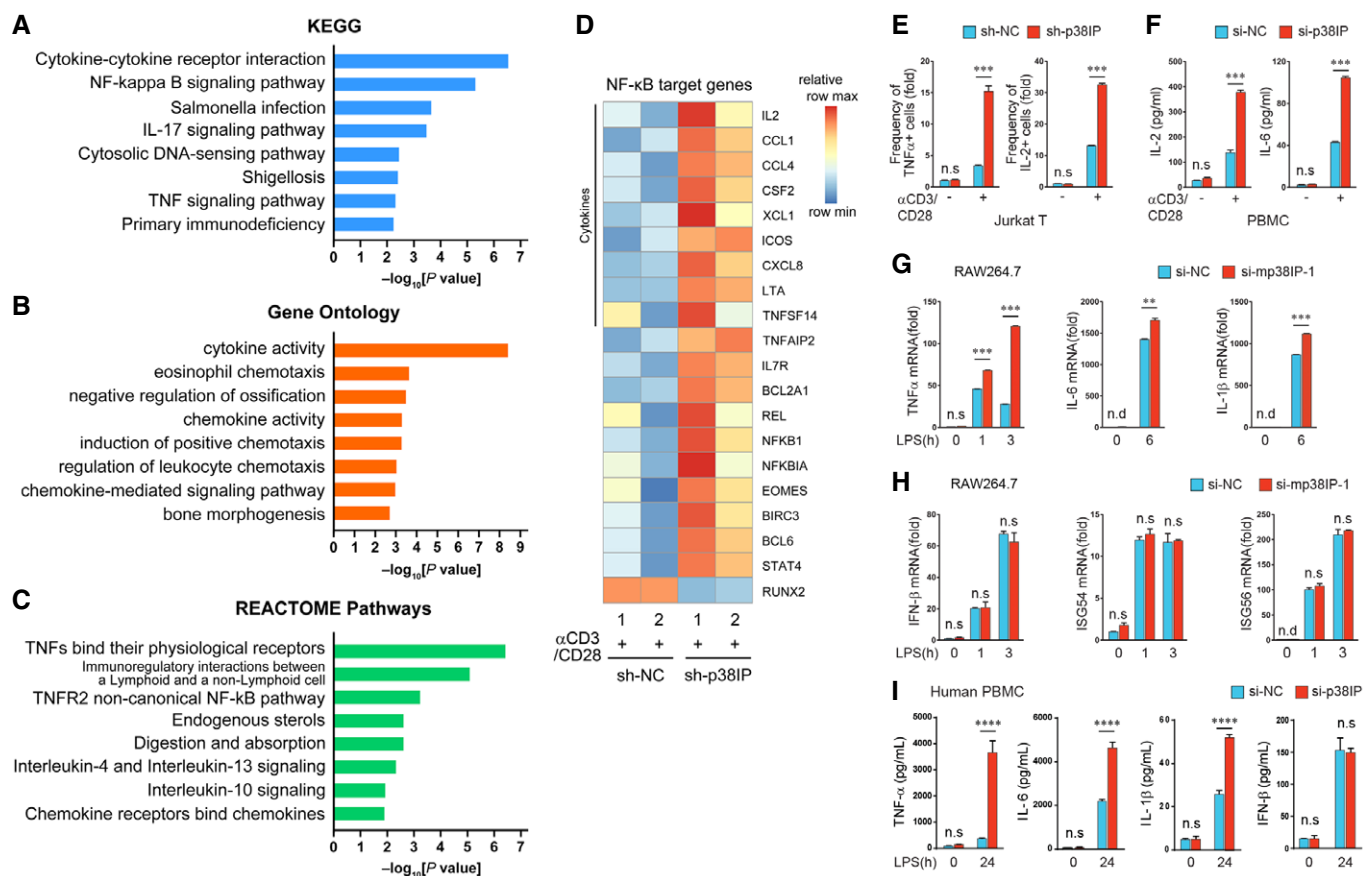
Figure 1. p38IP inhibits TCR- and LPS-induced cytokine production.

A–C Kyoto Encyclopedia of Genes and Genomes (KEGG), Gene Ontology (GO), and REACTOME Pathways (27.02.2019) enrichment analyses of differentially expressed genes in stimulated sh-NC vs. sh-p38IP Jurkat E6.1 T cells (fold change > 2, $P < 0.05$), showing the top 8 significantly enriched terms.

D Heatmap showing the expression change of representative NF-κB target genes from the genes with significantly changed expression (fold change > 2). The data represent the $\log_2$ (gene FPKM) normalized for each row. RNA-seq data are from 2 independent experiments.

E Intracellular cytokine staining assay of human TNF-α and IL-2 in sh-NC and sh-p38IP Jurkat E6.1 cells stimulated with 10 μg/ml anti-CD3 plus 2 μg/ml anti-CD28 for 6 h (average frequency of positive staining YFP$^+$ cells in sh-NC cells without stimulation = 1).

F ELISA analysis of IL-2 and IL-6 production in the culture supernatants of human PBMCs transfected with si-NC or si-p38IP, and then stimulated with 10 μg/ml anti-CD3 plus 10 μg/ml anti-CD28 (αCD3/CD28) for 24 h.

G, H Real-time PCR analysis of TNF-α, IL-6, and IL-1β (G) and of IFN-β, ISG54, and ISG56 (H) mRNA production in RAW264.7 cells transfected with si-NC and si-mp38IP-1 and then stimulated with 500 ng/ml LPS for the indicated times (average mRNA production in si-NC cells at 0 h = 1).

I ELISA analysis of TNF-α, IL-6, IL-1β, and IFN-β production in the culture supernatants of human PBMCs transfected with si-NC and si-p38IP and then stimulated with 1 μg/ml LPS for 24 h.

Data information: **$P < 0.01$, ***$P < 0.001$, ****$P < 0.0001$; n.d., not detectable; n.s, not significant (two-tailed unpaired t-test, mean and s.e.m.). Data are representatives of two (F, I) and three (E, G, H) independent experiments.

p38IP significantly enhanced the mRNA production of TNF-α, IL-6, and IL-1β in response to LPS stimulation (Fig 1G). LPS stimulation also activates IRF3 and type I interferon signaling through the adaptor protein TRIF [33], leading to the production of IFN-β and interferon-stimulated genes (ISGs). Interestingly, knockdown of p38IP had little effect on the mRNA production of IFN-β, ISG54, or ISG56 in RAW264.7 cells after LPS stimulation (Fig 1H). Similarly, knockdown of p38IP significantly elevated the protein production of TNF-α, IL-6, and IL-1β but not IFN-β (Fig EV1H). Intracellular cytokine staining analysis showed that si-mp38IP-2 enhanced the production of IL-6 in RAW264.7 cells stimulated with LPS, which was also observed with si-mp38IP-1 (Fig EV1I), excluding the off-target effects of RNA interference. To further validate the role of p38IP in LPS signaling, we expressed exogenous YFP-p38IP in THP-1 cells (a human monocytic cell line expressing TLR4) [34] and then treated them with LPS. We found that exogenous expression of YFP-p38IP strongly inhibited LPS-induced mRNA production of TNF-α, IL-6, and IL-1β (Fig EV1J), as well as protein production of TNF-α (Fig EV1K). Moreover, p38IP overexpression had no effect on IFN-β promoter-driven reporter gene expression (Fig EV1L). Further analysis showed that knockdown of p38IP in PBMCs significantly enhanced LPS-induced TNF-α, IL-6, and IL-1β production but had little effect on the production of IFN-β (Fig 1I).

Taken together, the above data demonstrate that p38IP negatively regulates TCR- or LPS-induced TNF-α, IL-6, IL-2, and IL-1β cytokine production but not LPS-induced IFN-β, ISG54, or ISG56 expression in T cells and/or in macrophages, probably through inhibition of NF-κB and p38 signaling.

p38IP is downregulated in RA pathogenesis

RA is a chronic autoimmune disease in which multiple joints become inflamed via infiltration of lymphocytes and mononuclear cells, activation of T cells and antigen-presenting cells, including macrophages, and production of pro-inflammatory cytokines [35]. Because the role of NF-κB and p38 as central checkpoints is well established in inflammation in general and in RA in particular [36–39], we reasoned that p38IP might have a role in RA pathogenesis. To test this hypothesis, PBMCs from 60 RA patients and 59 healthy donors were individually isolated and analyzed for p38IP expression levels. Intriguingly, we observed a downregulation of p38IP protein levels in RA patients compared to healthy donors (Fig EV2A). We also observed increased phosphorylation of p38 and decreased protein levels of IκBα in RA patients (Figs EV2B and C). Moreover, a significant negative correlation between p38IP protein levels and phospho-p38 ($P = 0.0004$, $r = -0.3198$) and a significant positive correlation between p38IP and IκBα protein levels ($P < 0.0001$, $r = 0.5996$) (Figs EV2D and E) were observed in most samples. Collectively, these data suggest that downregulation of p38IP may contribute to the elevated activation of p38 and NF-κB in RA, suggesting an inhibitory role for p38IP in RA pathogenesis.

Knockdown of p38IP enhances TCR- and LPS-induced activation of p38 and NF-κB

The results from RNA-seq and RA patients showed that p38IP may negatively regulate p38 MAPK and NF-κB, both of which are involved in the transcription of the *TNF-α, IL-1β, IL-2,* and *IL-6* genes [40,41]. Therefore, we determined whether and how p38IP regulated p38 MAPK and NF-κB activation in immune receptor signaling. First, we stimulated Jurkat E6.1 cells stably expressing sh-NC or sh-p38IP with anti-CD3/CD28 or PMA/ionomycin, and we found that knockdown of p38IP markedly enhanced TCR/CD28-induced p38, TAK1, IKKα/β, IκBα and p65 phosphorylation and PMA/ionomycin-induced p38 and IKK phosphorylation (Figs 2A and EV2F). Moreover, the phosphorylation of ERK and JNK was also increased in sh-p38IP cells (Fig 2A). Upon PMA/ionomycin stimulation, knockdown of p38IP promoted more cells to exhibit nuclear translocation of NF-κB p65, a hallmark of NF-κB activation (Figs 2B and EV2G), and increased NF-κB reporter gene expression (Fig 2C). Similarly, p38IP knockdown in RAW264.7 and T cells also obviously increased LPS-induced phosphorylation of TAK1, p38, IKKα/β, IκBα and p65, and the phosphorylation of ERK and JNK was only weakly increased by p38IP knockdown (Fig 2D). In contrast, LPS-induced phosphorylation of TBK1, which mediates LPS/IFN signaling [42], was similar in p38IP knockdown and control RAW264.7 cells (Fig 2E). We also found that p-TAB1 was increased in sh-p38IP cells following TCR stimulation (Fig EV2H), which is consistent with the finding that TAB1 is a substrate of p38 [43]. Further reporter gene assays showed that p38IP inhibited LPS-induced NF-κB activation but had little effect on LPS-induced interferon-sensitive response element (ISRE) activities (Fig EV2I). The above results combined with the results in Fig 1 suggest that p38IP negatively regulates both TCR- and LPS-induced p38 and NF-κB activation but not LPS-induced IRF signaling.

In addition to TCR and LPS, there are many other inducers of p38 and NF-κB, such as TNF, IL-1, and cellular stress.

Immunoblotting analysis revealed that TNF-α- and IL-1β-induced p38 and IKK phosphorylation were also enhanced in Jurkat E6.1 cells when p38IP was knocked down by sh-p38IP or the other three si-p38IP RNAs targeting three different regions of p38IP mRNA compared with the sh-NC group (Fig EV2J–M). Collectively, these results indicate that knockdown of endogenous p38IP enhances the activation of p38 and NF-κB induced by TCR, LPS, TNF-α, or IL-1β in T cells or macrophages.

p38IP inhibits TAK1 activation by competing with TABs for binding to TAK1 and interrupts unanchored K63-linked polyUb chain transfer from TAB2 to TAK1

We next explored the mechanisms underlying p38IP selective inhibition. TAK1 is a common central kinase for LPS-, TNF-α-, IL-1-, and TCR-induced p38 and NF-κB activation [9,10,44,45]; moreover, TAK1 is required for TLR3/TRIF-induced NF-κB but not IRF3 activation [9,46]. Therefore, the selective inhibitory function of p38IP we observed could result from p38IP targeting of TAK1 in these pathways. To test this hypothesis, we first performed a mass spectrometry analysis of the TAK1 protein complex in Jurkat T cells, and p38IP was detected (Figs 3A and EV3A). Then, we tested the association of p38IP and TAK1 in HEK 293T cells. Although TAK1 constitutively associates with TAB1 and TAB2 to form the TAK1-TAB complex [47], exogenously expressed p38IP was coimmunoprecipitated only with TAK1, not with TAB1 or TAB2 (Figs 3B and EV3B), indicating that p38IP interacted with TAK1 and that TAK1-p38IP and TAK1-TAB1-TAB2 were two distinct complexes in resting cells. In anti-TAK1 immunoprecipitates from resting Jurkat E6.1 T cells, we detected p38IP but not GCN5 (Fig EV3C), suggesting that p38IP associates with TAK1 in a GCN5/SAGA-independent manner.

We further examined whether and how p38IP regulates the kinase activity of TAK1. Sh-NC and sh-p38IP Jurkat E6.1 cells were stimulated with or without anti-CD3/CD28, and cell extracts were subjected to immunoprecipitation with anti-TAK1 antibody followed by an *in vitro* kinase assay using bacterially expressed truncated IKKβ as an exogenous substrate. In control cells, TAK1 activity was hardly detected before stimulation, whereas it was clearly detected after stimulation. However, TAK1 activity from unstimulated sh-p38IP cells was almost as strong as that from stimulated sh-NC cells and was markedly enhanced after stimulation (Fig 3C). This result indicates that p38IP could suppress the activity of TAK1. Given that the formation of the TAK1-TAB complex is essential for TAK1 activation and p38IP interacts with TAK1 but not TABs, it is quite reasonable to hypothesize that p38IP can suppress TAK1 activity by competing with TABs for TAK1 binding. In the competitive binding assay, exogenous expression of p38IP dose-dependently reduced the interactions of TAK1 with TAB2 (Fig 3D and E), TAB1 (Figs 3E and EV3D) and TAB3 (Fig EV3E). Moreover, the protein levels of TABs remained unchanged in cells transfected with increasing doses of p38IP (Figs 3D and E, and EV3D and E). Similarly, knockdown of p38IP enhanced the interaction between TAB2 and TAK1 in both resting and stimulated cells (Fig 3F). Collectively, these results indicate that p38IP suppresses TAK1 activity by competing with TABs for binding to TAK1, suggesting a balance between TAK1-p38IP and TAK1-TAB complexes in resting cells (Fig 3G).

As adaptors for TAK1 activation, TAB2/3 link K63-linked polyUb chains synthesized by the upstream E3 ligase with TAK1 to
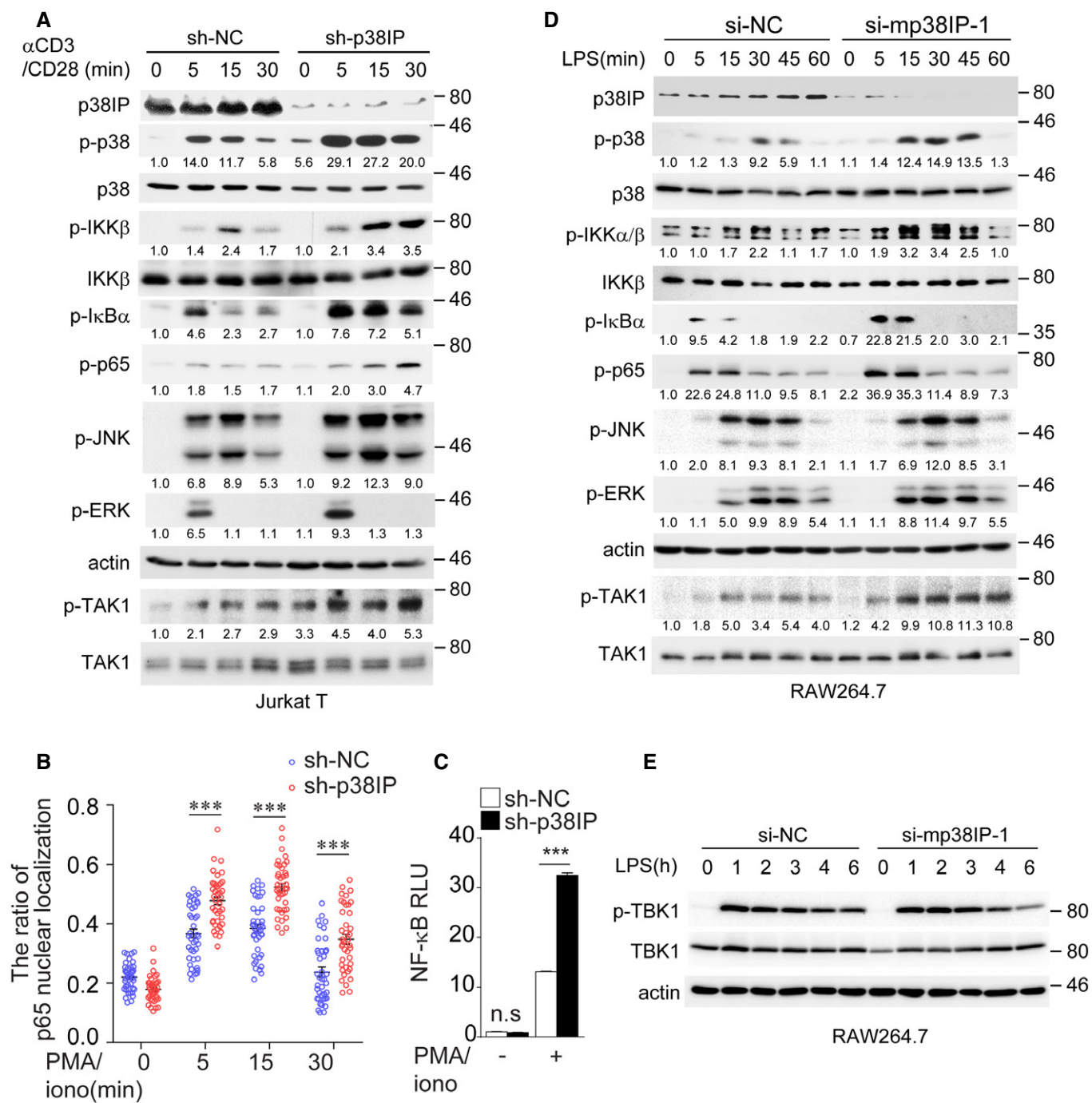
Figure 2. Knockdown of p38IP enhances TCR- and LPS-induced activation of p38 and NF-κB.

A   Immunoblot analysis with the indicated antibodies of total cell lysates of sh-NC and sh-p38IP Jurkat E6.1 cells stimulated with 10 μg/ml anti-CD3 plus 2 μg/ml anti-CD28 for the indicated times. Actin served as a loading control (throughout).

B   Statistical analysis of p65 nuclear translocation of sh-NC and sh-p38IP Jurkat E6.1 T cells stimulated with 50 ng/ml PMA plus 1 μM ionomycin for the indicated times. p65 nuclear translocation was indicated by the fluorescence intensities ratio between the nuclear p65 and the whole-cell p65 from each cell. ***$P < 0.001$ (two-tailed unpaired t-test, mean and s.e.m.).

C   Luciferase reporter assay of sh-NC and sh-p38IP Jurkat E6.1 cells transfected with NF-κB luc plus an internal control Renilla luciferase reporter for 36 h, followed by stimulation with (+) or without (−) 50 ng/ml PMA plus 1 μM ionomycin for 8 h. ***$P < 0.001$; n.s., not significant (two-tailed unpaired t-test, mean and s.e.m.).

D, E   Immunoblot analysis with the indicated antibodies of total cell lysates of RAW264.7 cells transfected with si-NC and si-mp38IP-1 and then stimulated with 500 ng/ml LPS for the indicated times.

Data information: Data in (A–E) are representatives of at least three independent experiments.
Source data are available online for this figure.

oligomerize and activate TAK1 [17–19,23,25]. These K63-linked polyUb chains are mostly unanchored [25]. It is unclear how TAB2/3 and TAK1 interact with the unanchored polyUb chains. Because p38IP reduced the association between TAB2 and TAK1, we next analyzed the effect of p38IP on the binding of polyUb chains to TAK1 and TAB2 under mildly denaturing conditions (lysis buffer containing 1% NP40) that do not interrupt non-covalent binding. As expected, exogenous expression of p38IP dramatically reduced TCR stimulation-induced binding of K63 polyUb chains to TAK1 (Fig 3H), whereas knockdown of p38IP enhanced TCR-induced K63 polyUb binding to TAK1 (Fig 3I), and accordingly, p38

phosphorylation and IκBα degradation were also enhanced (Fig 3I). Interestingly, in contrast to the inhibitory effect of p38IP on the binding of polyUb to TAK1, TCR-induced K63 polyUb binding to TAB2 was clearly enhanced by the exogenous expression of p38IP (Fig 3J), whereas it was significantly decreased by knockdown of endogenous p38IP (Fig 3K). These results demonstrate that p38IP only inhibited the induced binding of polyUb to TAK1 but not TAB2, while when p38IP expression increased or was knocked down, the binding of polyUb chains to TAK1 and TAB2 exhibited the opposite trends after stimulation. These results imply that when p38IP binds to TAK1 to disassemble the TAK1-TAB2 complex, it
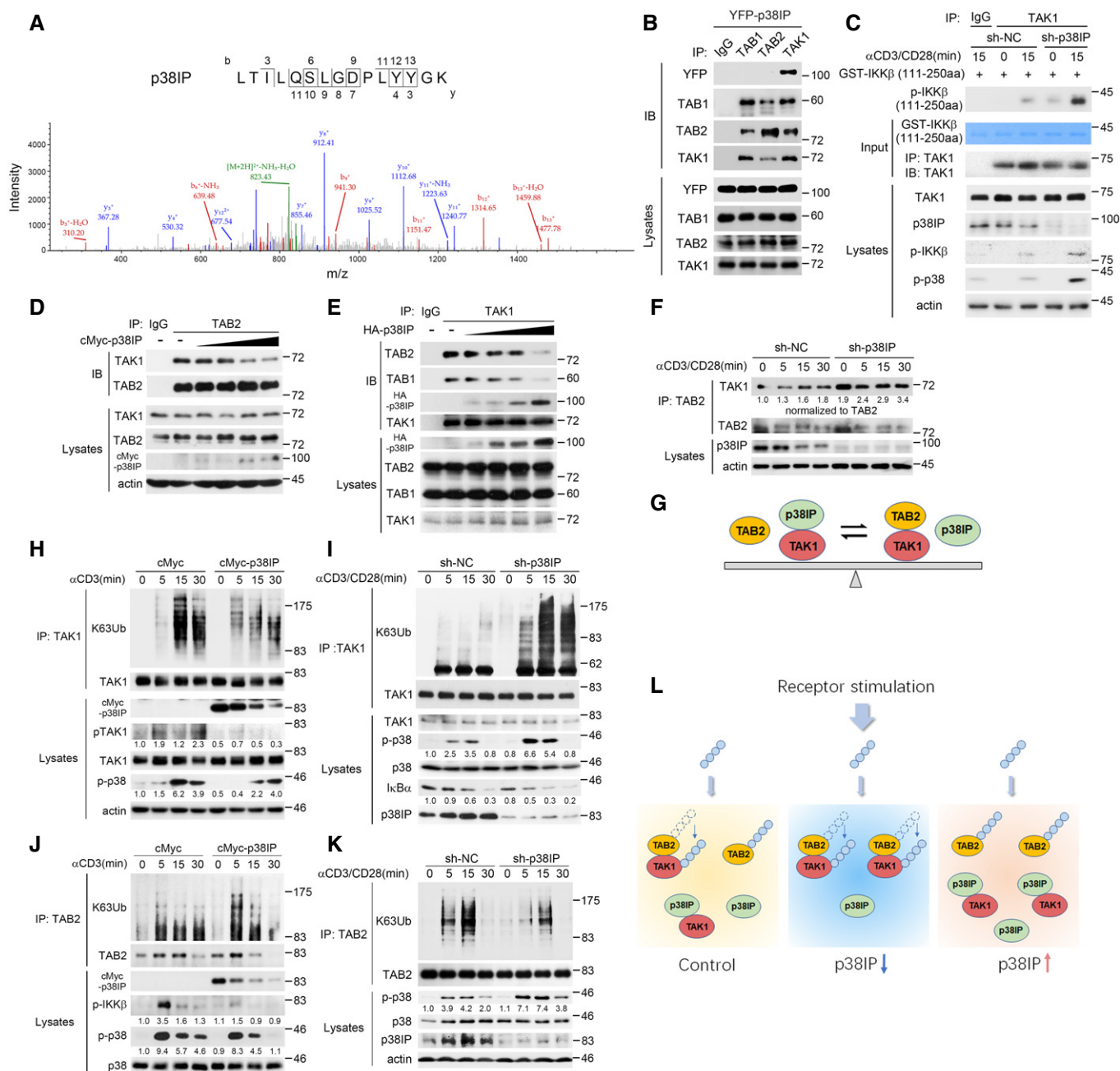

Figure 3.

◄

simultaneously blocks the K63-linked polyUb chain transfer from TAB2 to TAK1, suggesting that TAB2 should deliver the unanchored K63-linked polyUb chains to TAK1 to activate TAK1 and not solely bridge TAK1 to the polyUb chains bound by TAB2 [25]. Further knockdown of TAK1 led to an increase in TCR-induced binding of polyUb to TAB2 (Fig EV3F), confirming our hypothesis that TAB2 should act as a transfer of unanchored K63-linked polyUb chains *in vivo* and that TAK1 is the downstream acceptor for the ubiquitin chain. To further validate this conclusion, we analyzed the conjugated ubiquitination of TAK1 and TAB2 in control and p38IP-knockdown cells under stringent conditions (the cell lysates containing a final concentration of 1% SDS were heated for 10 min at 90°C to dissociate the proteins, followed by dilution and immunoprecipitation). Interestingly, while knockdown of p38IP still increased TAK1-conjugated ubiquitination, similar to the polyUb binding result in Fig 3I, TAB2-conjugated ubiquitination was not affected, different from polyUb binding result in Fig 3K (Fig EV3G). This result together with the findings presented in Fig 3H–K suggest that there is a transfer of unanchored polyUb chains from TAB2 to TAK1 that could be blocked by p38IP (Fig 3L), and the covalent ubiquitin conjugation of TAK1, but not TAB2, is also inhibited by p38IP.

Collectively, these data demonstrate that p38IP competes with TAB1/TAB2 for binding to TAK1, causing a balance between TAK1-p38IP and TAK1-TAB complexes in the cell, obstructing the unanchored polyUb chain relay from TAB2 to TAK1 and inhibiting covalent ubiquitination of TAK1.

p38IP dynamically interacts with TAK1 following stimulation

To understand the detailed mechanism underlying p38IP regulation of TAK1, we first investigated the temporal aspect of their association after stimulation. In resting T cells, p38IP constitutively associated with TAK1, similar to TAB2 (Fig 4A). Upon stimulation with anti-CD3/CD28 (Fig 4A), p38IP dramatically decreased its association with TAK1 at 2 min, whereas the association between TAB2 and TAK1 increased. After 5 min of stimulation, p38IP increased, whereas TAB2 decreased, its association with TAK1 (Fig 4A). Similar association dynamics of p38IP-TAK1 and TAK1-TAB2 or TAK1-TAB1 were also observed in human primary CD4$^+$ T cells stimulated with anti-CD3/CD28 (Fig EV4A), in Cos-7 cells with TNF-α (Fig EV4B), and in Jurkat E6.1 cells with LPS (Fig EV4C). In addition, after p38IP reassociated with TAK1, the stimulation-induced phosphorylation of IKKβ and p38 was gradually attenuated (Figs 4A and EV4A–C), while p-IKKβ showed a better negative temporal correlation with p38IP binding than p-p38 did (Figs 4A and EV4A), probably because p38 could also be phosphorylated by other kinases in addition to TAK1 in TCR signaling [48] and the regulation of p-p38 level still involves phosphatase. These results demonstrate that p38IP dynamically interacts with TAK1 and that the dynamic interaction of p38IP-TAK1 negatively correlates with that of TAB2-TAK1, in agreement with the above result that p38IP competes with TABs for TAK1 binding.

Next, we investigated how the dynamic interaction between p38IP and TAK1 was achieved. Given that stimulation induced the binding of K63-linked polyUb chains to TAK1-TABs and that the polyUb chains may transfer from TAB2 to TAK1, we speculated that the dynamic interaction may relate to the binding degree of polyUb with target proteins. To test this hypothesis, we constructed Ub-tagged TAB2 and TAK1 (Fig EV4D) and analyzed the effect of Ub modification on protein–protein interactions. As expected, TAK1 had a stronger association with Ub-tagged TAB2 than with TAB2 alone (Fig 4B), and p38IP had a stronger association with Ub-tagged TAK1 than with TAK1 alone (Figs 4C and EV4E), although the immunoprecipitated Flag-TAB2-Ub and Ub-TAK1-cMyc levels were much lower than those without Ub-tag (a large proportion of TAK1-cMyc was observed when Ub-TAK1-cMyc was overexpressed, which might be caused by deubiquitination) (Figs 4B and C, and EV4E). Moreover, in contrast to TAK1 alone, Ub-tagged TAK1 showed
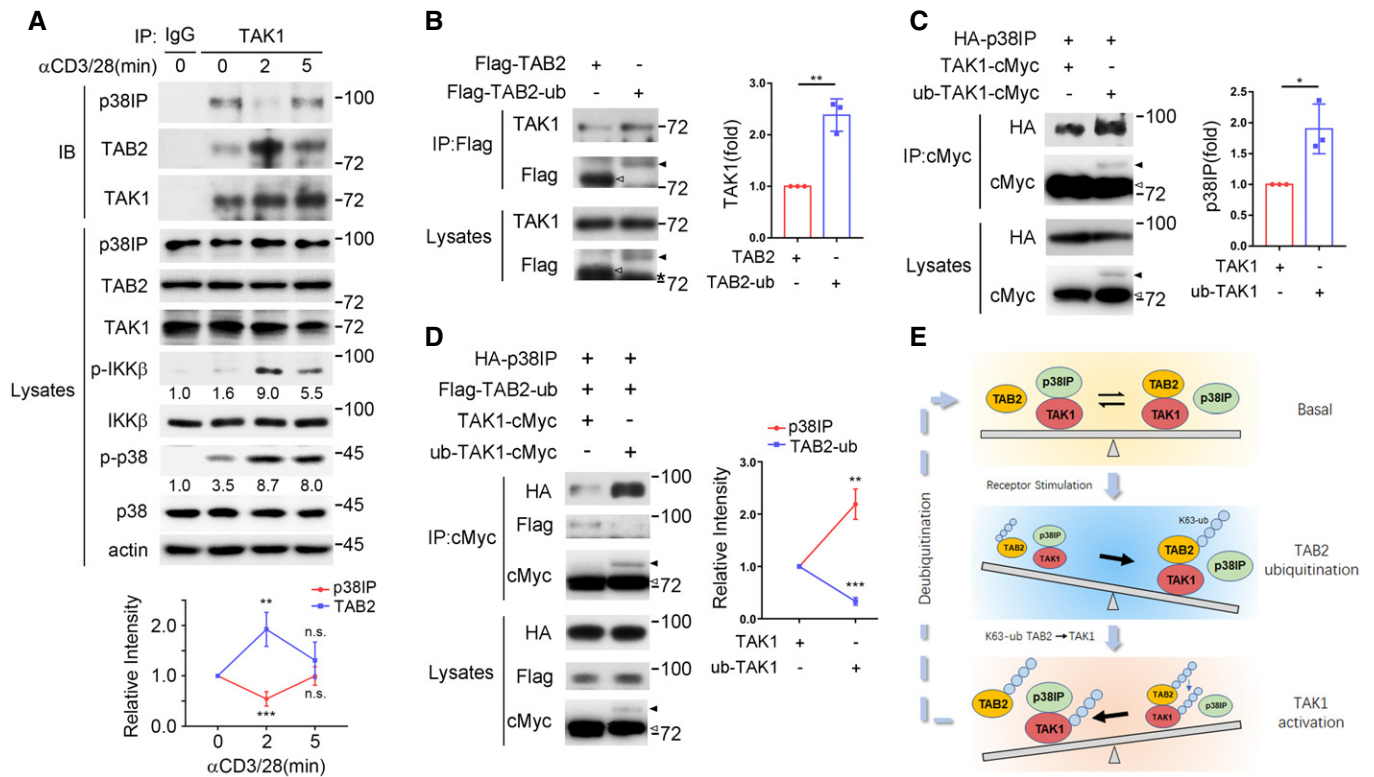
Figure 4. p38IP dynamically interacts with TAK1 following stimulation.

A   Jurkat E6.1 T cells were stimulated with 10 μg/ml anti-CD3 and 2 μg/ml anti-CD28 for the indicated times, and the cell lysates were immunoprecipitated and immunoblotted as indicated. The relative intensity of the IP bands was quantified by densitometry and is shown below the graph.

B   HEK293T cells transfected with Flag-tagged TAB2 (open arrow) or TAB2-ub (solid arrow) were lysed and immunoprecipitated with anti-Flag, and then immunoblotted with the indicated antibodies. The asterisk indicates a non-specific band. The relative intensity of the IP bands was quantified by densitometry and is presented in the right.

C   HEK293T cells co-transfected with HA-tagged p38IP together with cMyc-tagged TAK1 (open arrow) or ub-TAK1 (solid arrow) were lysed and immunoprecipitated with anti-cMyc, and then immunoblotted with the indicated antibodies. Asterisk indicates non-specific bands. The relative intensity of the IP bands was quantified by densitometry and is presented in the right.

D   HEK293T cells co-transfected with HA-tagged p38IP, Flag-tagged TAB2-ub, together with cMyc-tagged TAK1 (open arrow) or ub-TAK1 (solid arrow), were lysed and immunoprecipitated with anti-cMyc, and then immunoblotted with the indicated antibodies. The relative intensity of the IP bands was quantified by densitometry and is presented in the right.

E   Schematic of dynamic association between p38IP and TAK1 after stimulation.

Data information: Data are representatives of three (B–D) and four (A) independent experiments. *$P < 0.05$, **$P < 0.01$, ***$P < 0.001$; n.s., not significant (two-tailed unpaired t-test, mean and s.e.m.).
Source data are available online for this figure.

---

much stronger binding affinity with p38IP than with Ub-tagged TAB2 (Fig 4D). Combining the above results that TAK1 and p38IP, respectively, had a higher binding affinity for polyUb-bound TAB2 and TAK1 with the possible polyUb chain transfer model, we propose the dynamic interaction model in Fig 4E, which could explain why p38IP dissociated from and reassociated with TAK1 after stimulation.

In vitro analysis of K63-linked polyUb chain binding and transferring and changing protein binding affinity

To confirm our conclusions in Fig 4E, we further performed *in vitro* polyUb chain binding analysis. In our working model, TAK1 was proposed to bind to K63-linked polyUb chains. Thus, we first tested whether TAK1 could bind to unanchored polyUb chains by an

in vitro GST pull-down assay, with NEMO serving as a positive control and the NEMO L329P mutant as a negative control [49]. We found that GST-fused TAK1 protein could pull down many more penta-Ub to hepta-Ub chains than NEMO did (Fig 5A and Appendix Fig S1). The ubiquitin-associated domain of NEMO (UBAN domain) consists of a coiled-coil domain and a leucine zipper domain [50]. Interestingly, the TAK1 531–595 aa region contains a coiled-coil domain (531–582 aa) with a very high confidence score and a possible leucine zipper domain (570–595 aa) with a relatively low score predicted with Phyre2 3D modeling, implying that the TAK1 531–595 aa region might be a UBA domain. We then attempted to map the possible UBA domain of TAK1 by constructing various GST-TAK1 truncated mutants and a TAK1 L575P mutant that mimics the mutation of NEMO L329, the key leucine responsible for NEMO polyUb binding [49]. Nevertheless, we could not

conclude which region is responsible for TAK1 polyUb binding from the GST pull-down assay because all the mutants associated with polyUb chains and full-length TAK1 had the best association (Fig 5A). Hence, TAK1 can bind to polyUb chains, and the detailed biochemical mechanism underlying this binding remains to be further studies.

Next, we tested the K63-linked polyUb chain transfer model *in vitro*. The strategy we employed is shown in Fig 5B: GST-TAB2 on glutathione (GSH)-Sepharose beads was pre-incubated with K63-linked polyUb chains and then eluted from the beads, followed by incubation with purified GST-TAK1 (treatment a) or with GST-TAK1 and GST-p38IP proteins simultaneously (treatment b) or sequentially (treatment c) (Fig 5B). Then, the incubated mixture was immunoprecipitated separately with anti-TAB2 and anti-TAK1. The immunoblot analysis revealed that after incubation with K63 polyUb chains, TAB2 bound to polyUb chains (Fig 5C, lane 2), and further incubation with TAK1 decreased this binding to TAB2 (Fig 5C, treatment a), while the polyUb binding to incubated TAK1 was clearly detected (Fig 5D, treatment a), indicating the transfer of polyUb chains from TAB2 to TAK1. This transfer was partially blocked when p38IP and TAK1 were co-added as shown in treatment b compared with treatment a (Fig 5C–E). Nevertheless, p38IP could barely block this transfer when it was added 1 h after TAB2-TAK1 incubation as shown in treatment c, compared with the transfer in treatment b (Fig 5C–E), meaning that p38IP could not reverse the already occurred ubiquitin transfer. The transfer results *in vitro* are in line with the *in vivo* results in Fig 3, confirming the transfer of K63-linked polyUb chains from TAB2 to TAK1.

Next, we performed *in vitro* protein binding assays to determine the ubiquitin-mediated binding affinity in our dynamic binding model. Consistent with the results in cells (Fig 4), TAK1 had a much stronger binding with polyUb-bound TAB2 than with TAB2 alone, while the binding affinity between both polyUb-bound TAK1 and TAB2 was similar to that between TAK1 and polyUb-bound TAB2 (Fig 5F). Similarly, p38IP had a stronger association with polyUb-bound TAK1 than with TAK1 alone (Fig 5G).

Taken together, the above data confirm the polyUb chain transfer and the higher binding affinity of TAK1 and p38IP for polyUb-bound TAB2 and TAK1, respectively, which lead to the dynamic interaction between p38IP and TAK1 upon stimulation.

The T1B (215–275 aa region) of p38IP is responsible for its interaction with TAK1

To identify the region within p38IP responsible for the TAK1 interaction, we first generated two truncated mutants, p38IP-N (aa residues 1–381) and p38IP-C (aa residues 380–733). By immunoprecipitation, we found that p38IP-N, but not p38IP-C, could interact with TAK1 (Appendix Fig S2A). To map the essential TAK1 binding region within p38IP-N, a series of truncated N-terminal mutants were then generated following the rules of avoiding disruption of protein folding (Fig 6A), and the coimmunoprecipitation results showed that only the mutants containing the 215–275 aa residues (red box indicated in Fig 6A) could associate with TAK1 (Fig 6B), indicating that the 215–275 aa region within p38IP is required for the interaction with TAK1. Further immunoprecipitation analyses using a series of truncated C-terminal mutants of p38IP showed that only when the C-terminus of a mutant was extended to include the

215–275 aa region could it bind to TAK1 (Appendix Fig S2B). In addition, sequence alignment indicated that this 215–275 aa region is conserved among species from *Drosophila* to *Homo sapiens* (Appendix Table S2). Structural modeling showed that this region could fold into three α-helixes to generate the protein domain core. Thus, we named this region the TAK1 binding domain (T1B). By superimposing the predicted 3D structure of p38IP-T1B onto a previously characterized TAK1 structure (PDB: 5V5N [51]), we generated a docking model for p38IP-T1B and TAK1 (Fig 6C), which suggested that T1B itself could bind with TAK1. Indeed, GST-tagged T1B could pull down endogenous TAK1 in a GST pull-down analysis, and reciprocally, YFP-tagged T1B could be immunoprecipitated by endogenous TAK1 (Fig 6D and E), indicating that T1B alone is sufficient for p38IP binding to TAK1. Collectively, these results demonstrate that T1B of p38IP is responsible for p38IP binding to TAK1.

By comparing the TAK1-T1B docking model with the TAK1-TAB 1 crystal structure (PDB: 2EVA), we found that the T1B interaction region of TAK1 partially overlapped with the TAB1 binding pocket (Appendix Fig S2C), indicating that T1B alone could interrupt the TAK1-TABs association. As expected, exogenous expression of p38IP-N and p38IP-T1B reduced the interaction between TAB1/TAB2 and TAK1 in a dose-dependent manner (Appendix Fig S2D and E). Not surprisingly, exogenous expression of p38IP-C had no effect on the interaction between TAK1 and TAB1/TAB2 (Appendix Fig S2F).

Next, we determined whether p38IP-T1B could carry out the inhibitory function of p38IP in TAK1-mediated NF-κB and p38 activation. The immunoprecipitation and immunoblot analysis revealed that under mildly denaturing conditions, exogenous p38IP-T1B expression reduced CD3-induced binding of polyUb chains to TAK1 in Jurkat T cells (Fig 6F) but increased the induced binding of polyUb chains to TAB2 (Appendix Fig S2G), consistent with the results presented in Fig 4E and again supporting our hypothesis that ubiquitin chains transfer from TAB2 to TAK1. Moreover, exogenous p38IP-T1B expression in primary human PBMCs inhibited TCR-induced phosphorylation of IKKα/β, IκBα, and p38 (Fig 6G) and attenuated TCR-induced TNF-α and IL-2 production (Fig 6H). Taken together, these results demonstrate that p38IP-T1B mediates the p38IP interaction with TAK1 to interfere with the assembly of the TAK1-TAB complex, which in turn inhibits TCR-induced NF-κB and p38 activation.

p38IP scaffolds USP4 to deubiquitinate TAK1

Although, similar to p38IP, p38IP-T1B inhibited TCR-induced binding of polyUb chains to TAK1, NF-κB and p38 activation and cytokine production (Fig 6F–H), p38IP had a much stronger inhibitory effect than T1B on LPS-induced cytokine production (Appendix Fig S2H), even though the exogenous protein expression level of p38IP was much lower than that of p38IP-T1B (Appendix Fig S2H). This result indicated that p38IP is more efficient than p38IP-T1B in the inhibition of TAK1 activation, suggesting that p38IP has other mechanisms of inhibiting TAK1 in addition to interfering with TAK1-TAB complex assembly. Indeed, the above immunoblot analysis results showed that under stringent conditions, knockdown of p38IP also increased TAK1-conjugated ubiquitination (Fig EV3G). Therefore, we examined whether p38IP could function as an adaptor to recruit

a DUB to deubiquitinate TAK1. The DUBs CYLD [52,53], USP4 [54,55], and USP18 [5,56], which have been reported to deubiquitinate the K63-linked polyubiquitination of TAK1, USP22, which coexists with p38IP in the SAGA complex [57], and USP3, which can remove K63-linked polyUb chains from RIG-I [58], were tested for their interaction with p38IP. We found that USP4, but not USP3, 22, or 18, was associated with YFP-p38IP (Figs 7A and EV5A). In addition, CYLD did not associate with YFP-p38IP either, but clearly, CYLD interacted with TAK1 (Fig EV5B), as previously reported [52]. Next, we assessed whether p38IP expression could promote USP4 binding to TAK1. While both USP4 and USP22 were associated with

TAK1 (Figs 7B and EV5C), exogenous expression of p38IP dramatically increased the interaction between TAK1 and USP4 (Fig 7B) but had no effect on the TAK1-USP22 interaction (Fig EV5C). These results suggest that p38IP specifically binds to USP4 and facilitates its recruitment to the TAK1 complex. Moreover, the *in vivo* deubiquitination assay under stringent conditions revealed that the expression of only Flag-USP4, Flag-USP22, or Flag-USP3 reduced the K63-linked polyubiquitination of TAK1 to a certain degree, while co-expression with YFP-p38IP dramatically enhanced the deubiquitination ability of USP4 but not that of USP22 or USP3 (Fig 7C). The *in vitro* deubiquitination assay with purified Flag-p38IP or
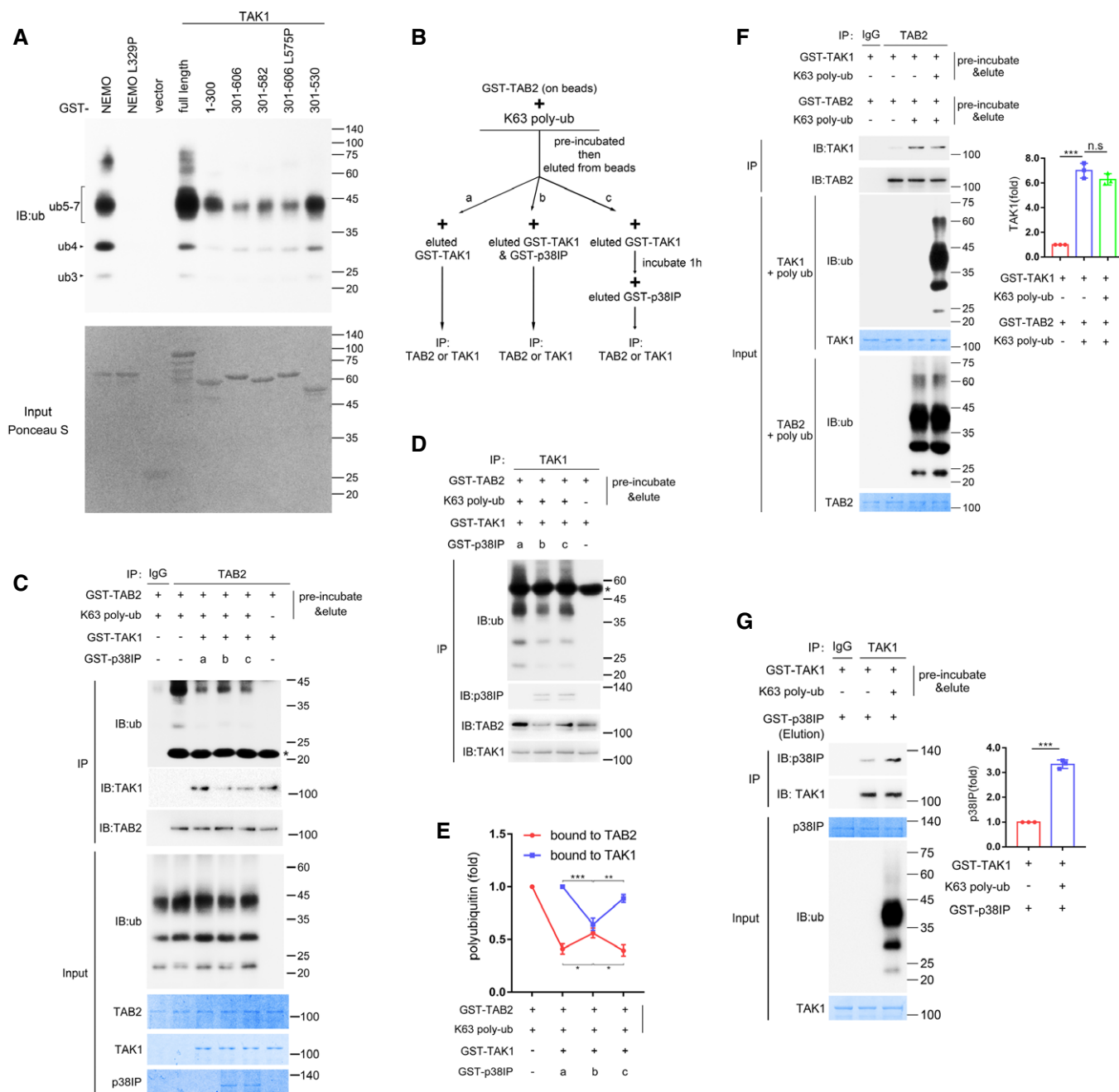

Figure 5.

◄

Figure 5. *In vitro* analysis of K63-linked polyUb binding, transferring and influencing protein binding affinity.

A   GSH-Sepharose bead-immobilized full-length or truncated GST-TAK1 proteins were incubated with K63-linked polyUb chains in 300 µl binding buffer, followed by washing and resolving in SDS–PAGE, and then immunoblotted with anti-ub. GST-fused NEMO served as positive control and NEMO L329P mutant as negative control. The blotted membrane was stained with Ponceau S to demonstrate the amount of the input GST-fused proteins (lower panel).

B   Strategy for *in vitro* polyUb transfer experiments.

C, D Immobilized GST-TAB2 was pre-incubated with K63-linked polyUb chains and then eluted from beads, followed by incubation with eluted GST-TAK1 and GST-p38IP as shown in (B). Incubation mixture was immunoprecipitated with anti-TAB2 or anti-TAK1, and then immunoblotted with anti-ub, anti-TAB2, anti-TAK1, and anti-p38IP.

E   Statistical analysis of polyUb binding to TAB2 or TAK1 in (C and D). *$P < 0.05$, **$P < 0.01$, ***$P < 0.001$ (two-tailed unpaired *t*-test, mean and s.e.m.).

F   Immobilized GST-TAB2 and GST-TAK1 were, respectively, pre-incubated with K63-linked polyUb chains or not as indicated, then eluted from beads, followed by coincubation as indicated. Incubation mixture was immunoprecipitated with anti-TAB2, and then immunoblotted with anti-TAB2 and anti-TAK1. The relative intensity of immunoprecipitated TAK1 was calculated and shown in the right. ***$P < 0.001$; n.s., not significant (two-tailed unpaired *t*-test, mean and s.e.m.).

G   Immobilized GST-TAK1 was pre-incubated with K63-linked polyUb chains or not, then eluted from beads, followed by incubation with eluted GST-p38IP. Incubation mixture was immunoprecipitated with anti-TAK1, and then immunoblotted with anti-TAK1 and anti-p38IP. The relative intensity of immunoprecipitated p38IP was calculated and shown in the right. ***$P < 0.001$ (two-tailed unpaired *t*-test, mean and s.e.m.).

Data information: Data are representatives of at least three independent experiments.
Source data are available online for this figure.

Flag-USP4 protein showed that although neither could reverse the ubiquitination of TAK1, together they could strongly deubiquitinate TAK1 (Fig 7D). Furthermore, in T cells, while anti-CD3/CD28-induced TAK1 ubiquitination was strongly blocked by exogenous USP4 expression, it was dramatically enhanced by the knockdown of p38IP, and this enhancement could no longer be blocked by exogenous USP4 expression (Fig 7E). In contrast, exogenous expression of USP22 blocked anti-CD3/CD28-induced TAK1 ubiquitination in both control and p38IP knockdown T cells (Fig EV5D). These results suggested that p38IP is required for USP4-mediated, but not USP22-mediated, deubiquitination of TAK1. Moreover, both the associations of USP4 with p38IP and with TAK1 were weakly detected in resting cells and dramatically promoted upon TCR or LPS stimulation (Figs 7F and EV5E), while the binding affinities for p38IP with Ub-TAK1 and for USP4 with Ub-TAK1 increased to a similar extent compared to their affinities with TAK1 (Fig EV5F). Furthermore, the TCR-enhanced USP4-TAK1 interaction was dramatically diminished in p38IP knockdown T cells (Fig 7G). These results indicated that stimulation-enhanced recruitment of USP4 to TAK1 is dependent on p38IP with a higher affinity to ubiquitinated TAK1. The stimulation-increased association between USP4 and p38IP may involve their stimulation-induced modification, and TCR was found to induce phosphorylation of p38IP (Fig EV5G). The above results demonstrate that USP4 is specifically recruited by p38IP to deubiquitinate TAK1.

To determine which region was responsible for p38IP binding to USP4, we co-transfected truncated p38IP mutants with USP4 in HEK 293T cells and then assessed their interaction. Through a stepwise mapping approach, we found that the 1–157 aa region of p38IP was the USP4-binding domain (U4B) (Figs 7H and EV5H). Exogenous expression of p38IP-U4B could not efficiently inhibit the TCR-induced ubiquitination of TAK1 as T1B or full-length p38IP did in Jurkat T cells (under stringent conditions) (Fig EV5I), consistent with the finding that p38IP-U4B lacked the TAK1 binding domain T1B.

Next, we used structural modeling to understand why p38IP specifically recruits USP4 but not CYLD. Template-based modeling analysis showed that the p47 SEP domain (after shp1, eyc and p47) could be the modeling template for the p38IP U4B domain (Fig EV5J). The p47 SEP domain adopts a fold with a βββααβ secondary structure arrangement, where β4 packs parallel to β1

(Fig EV5J). It has been reported that the human p47 SEP domain could reversibly associate with cysteine protease cathepsin L, and residues located in the turn between β1 and β2, in the loop following β3, and near the flexible C-terminus of the SEP domain are the binding sites between them [59], indicating that the amino acids located in these regions of the SEP domain are responsible for protein–protein interactions. Multiple sequence alignment showed that the residues critical for folding into βββααβ are conserved in p38IP U4B among various species (Fig EV5K). Using the Phyre2 server [60], we generated the 3D structure of p38IP-U4B. By superimposing the predicted 3D structure of p38IP-U4B onto a previously characterized USP4 D1D2 structure (PDB: 2Y6E), we generated the docking model for p38IP-U4B and USP4 (Fig EV5L). Indeed, the conserved residues of p38IP-U4B (Asp 99, Tyr 107, Ala 118, Asp 148, Tyr 149, and Arg 150), which are in the loop following β3 and near the flexible C-terminus of the U4B domain, are located in the cavity formed by the USP domain of USP4 (Fig 7I). We next compared the docking model of p38IP-USP4 with that of p38IP-CYLD. The docking model of p38IP-U4B and USP4 showed that the fingers subdomain of USP4 forms a cavity-like structure that could accommodate several residues of the p38IP-U4B C-terminus (Fig 7J, left). However, the finger subdomain of the CYLD USP domain has each "finger" greatly reduced [61]; thus, it cannot accommodate the U4B C-terminus as USP4 does (Fig 7J, right). The structural difference between the fingers subdomains of USP4 and CYLD could lead to the specific binding of p38IP to USP4 but not to CYLD.

Taken together, these findings suggest that p38IP inhibits TAK1 activation through a dual mechanism: interrupting TAK1 complex assembly via its T1B domain and scaffolding the association between USP4 and TAK1 via its U4B domain (Fig EV5M). Based on our findings, we propose a working model for the p38IP negative regulation of TCR/LPS signaling (Fig 7K).

Discussion

In this study, we uncovered that p38IP is a negative regulator of TCR/LPS signaling and is downregulated in PBMCs of RA patients. We demonstrated that p38IP suppresses TAK1 activation and that there is an intrinsic p38IP-TAK1 complex and a balance between

A

YFP-p38IP-N	1		381
YFP-p38IP-N1	74		381
YFP-p38IP-N2	158		381
YFP-p38IP-N3	215	T1B	381
YFP-p38IP-N4	276		381
YFP-p38IP-N5	318		381
YFP-p38IP 1-214	1		214
YFP-p38IP 1-275	1	T1B	275
YFP-p38IP-C	380		733

B

C

p38IP-T1B
TAK1

D

E

HEK293T
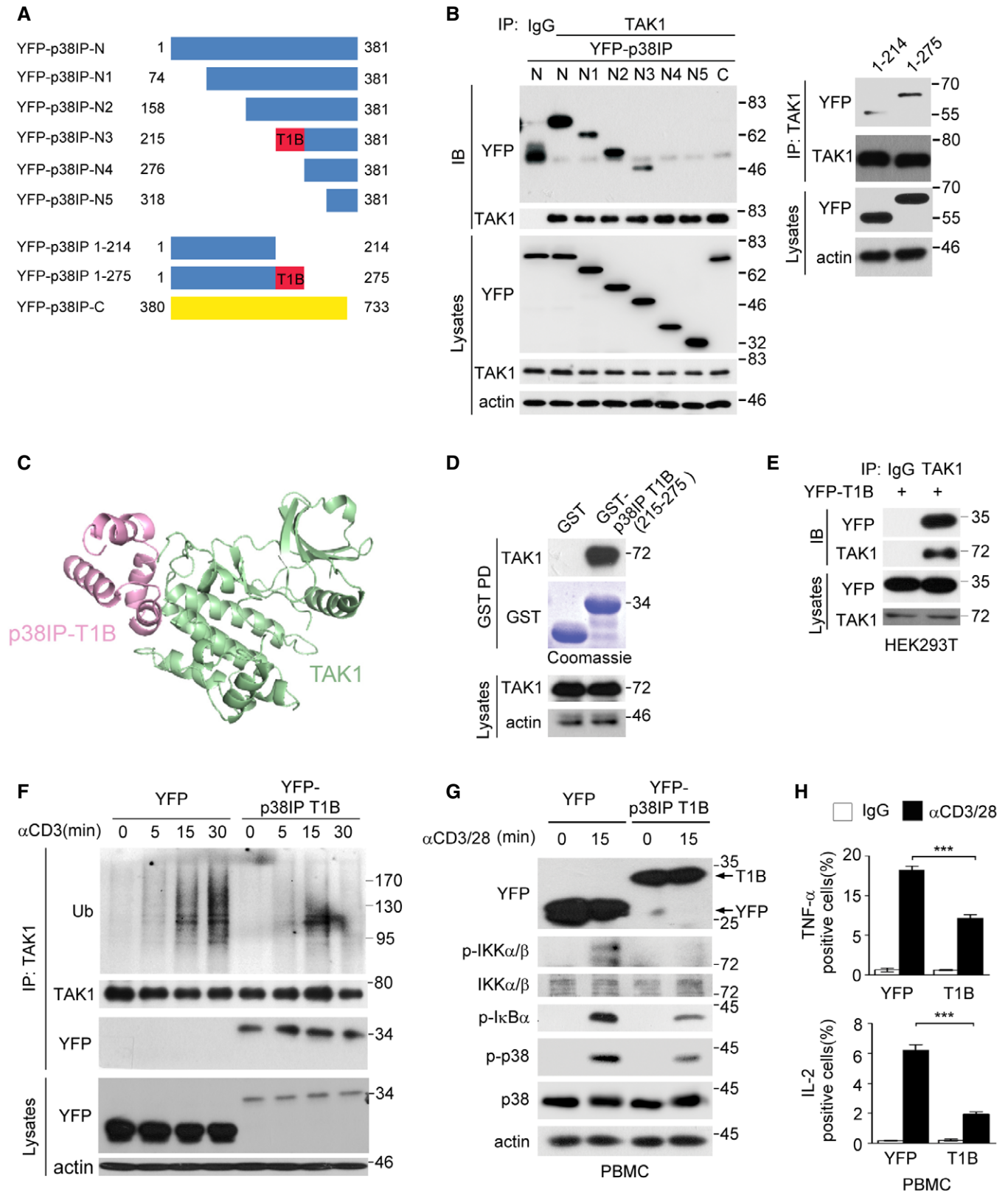
F

G

PBMC

H

Figure 6.

Figure 6. The T1B (215–275 aa region) of p38IP is responsible for its interaction with TAK1.

A   Schematic diagram of the truncations of p38IP, in which the numbers indicate the residues of the truncations and the red box indicates T1B.

B   HEK293T cells transfected with N-terminal (left panels) or C-terminal (right panels) deletion mutants of p38IP as indicated in (A) were lysed after 24 h transfection and immunoprecipitated with IgG or anti-TAK1, followed by incubation with protein G beads, and then immunoblotted with anti-YFP and anti-TAK1.

C   Ribbon representation of a model structure of the p38IP-T1B (pink) and TAK1 (green).

D   GST pull-down assay. 3 µg recombinant GST-T1B protein which immobilized on glutathione-Sepharose beads was incubated with the cell lysates that obtained by adding 1 ml lysis buffer to the HEK293T cells in 10 cm cell culture dish with a final protein concentration around 1 µg/µl, after 4 h incubation, washed beads with cell lysis buffer five times, and subjected to SDS–PAGE for immunoblotting with anti-TAK1.

E   HEK293T cells transfected with YFP-p38IP T1B were lysed after 24 h of transfection and immunoprecipitated with IgG or anti-TAK1, followed by incubation with protein G beads, and then immunoblotted with anti-YFP and anti-TAK1.

F   Jurkat TAg cells transfected with YFP vector or YFP-T1B were stimulated with 10 µg/ml anti-CD3 for indicated times, and then lysed and immunoprecipitated with anti-TAK1, followed by immunoblotting with the indicated antibodies.

G   Primary human PBMCs transfected with YFP vector or YFP-T1Bwere stimulated with 10 µg/ml anti-CD3 plus 10 µg/ml anti-CD28 for the indicated times, then lysed and analyzed by immunoblotting.

H   Intracellular cytokine staining analysis of TNF-α (upper) and IL-2 (lower) in primary human PBMCs transfected and stimulated as in (F) for 3 h (TNF-α) and 8 h (IL-2).

Data information: Data are representatives of three independent experiments. ***$P < 0.001$, (two-tailed unpaired t-test, mean and s.e.m.).

Source data are available online for this figure.

p38IP-TAK1 and TAB-TAK1 complexes (Fig 3G). We found that K63-linked polyUb chains are transferred as batons from TAB2 to TAK1 (Fig 3L). p38IP dynamically associates with TAK1 during stimulation because of the transfer of polyUb chains from TAB2 to TAK1 and the higher binding affinity of p38IP and TAK1 to polyUb-bound TAK1 and TAB2, respectively (Fig 4E). We also found that p38IP specifically recruits the deubiquitinase USP4 but not CYLD to deubiquitinate TAK1 and performed a structural analysis with 3D docking modeling. These findings establish p38IP as an intrinsic negative counterpart of TABs and a scaffold protein for USP4 and suggest a transfer model for unanchored polyUb chains. We summarize these findings in a schematic in Fig 7K.

Dynamic responses substantially increase the accuracy of biochemical signaling networks [62]. TAK1 is the central kinase of receptor-mediated NF-κB and MAPK signaling, yet its dynamic regulation is poorly understood. In this study, we found that p38IP dynamically interacts with TAK1 according to the polyUb-bound status of TAK1 upon receptor stimulation. Based on our findings, we propose a model for this dynamic binding: In resting T cells, there is a balance between TAK1-TAB2 and TAK1-p38IP complexes; stimulation-induced binding of polyUb to TAB2 promotes TAK1 interaction with polyUb-bound TAB2, thus decreasing the p38IP-TAK1 interaction, and then the transfer of polyUb chains from TAB2 to TAK1 increases p38IP binding with polyUb-bound TAK1, interfering with TAB2-TAK1 binding (Fig 4E). The dynamic regulation of TAK1 and the hyperphosphorylation of TAK1 caused by p38IP knockdown indicate that p38IP is an intrinsic sensor of TAK1 activity, facilitating the accurate activation of TAK1. Of note, multiple regulatory mechanisms may be involved in the dynamic regulation of TAK1, such as p38 inhibiting TAK1 activation by phosphorylating TAB1 [43].

It has been demonstrated that TAB2/3 activates TAK1 by preferentially binding to unanchored K63-linked polyUb chains synthesized by TRAF6, thus bringing together TAK1 and these polyUb chains to induce a conformational change in TAK1 inducing its activation [20]. To date, the function of unanchored K63-linked polyUb chains and their regulatory mechanism are still unclear. It is thought that TAK1 and TAB2/3 simultaneously bind to the same unanchored K63-linked polyUb chains [21,25]. However, while TAB2 uses its NZF domain to bind the specific motifs of the proximal ubiquitin and the distal ubiquitin [18,25], it is unknown how TAK1

interacts with the same unanchored K63-linked polyUb chains both simultaneously and specifically. Our transfer model suggests that these unanchored polyUb chains are transferred as batons from TAB2 to TAK1 rather than being bound by TAB2 and TAK1 simultaneously (Fig 3L). In this model, TAK1 is predicted to bind with K63 polyUb chains itself, and we did find that TAK1 itself bound with K63 polyUb chains in the absence of TAB2, although the exact underlying biochemical mechanism is currently unknown. The transfer of unanchored K63-linked polyUb chains should favor the conformational change of TAK1 without being restricted by TAB2 and the dynamically precise regulation of TAK1, thus achieving accurate signal transduction. Directional transfer could make these ubiquitin chains become real "second messengers" [63].

Several DUBs have been demonstrated to target TAK1, including CYLD, USP4, and USP18 [21], showing not only functional overlap but also specificities. For example, *CYLD* deficiency does not alter the level of the LPS-stimulated activation of IKKβ in macrophages [52], USP18 is differentially expressed in different T helper cells and is only essential for Th17 cell differentiation [5], and USP4 binding to TAK1 is stimulation-dependent [54]. However, the molecular mechanisms underlying their specificities remain largely unclear. In this study, we found that USP4, but not CYLD or USP18, binds to p38IP, and stimulation promoted the association of USP4 with TAK1 due to the higher affinities between p38IP and polyUb-bound TAK1 and between p38IP and USP4 after stimulation, indicating that p38IP is a specific adaptor for USP4 targeting TAK1. Further 3D docking model analysis revealed that the specificity of p38IP to USP4 probably results from the structural differences between the finger subdomains of USP4 and CYLD for docking the p38IP U4B domain. Moreover, our finding that USP4 inhibits TCR-induced covalent ubiquitination of TAK1 combined with the reported USP4 inhibition of TNFα-, IL-1β-, and LPS-induced NF-κB [54] indicates that USP4 and p38IP have a similar physiological regulatory pattern and an intrinsic relationship. Activation of NF-κB involves at least three types of ubiquitin chains, K63, M1, and K48 linkages, and CYLD is a K63/M1 linkage-specific DUB [64]. A recent study demonstrated that K48-K63 branched ubiquitin linkages are abundant in cells and are involved in TAK1 activation [65]. Interestingly, this branched ubiquitin chain counteracts CYLD-mediated K63 deubiquitination but could be cleaved by the universal DUB USP2 [65]. USP4 is structurally very close to USP2 [66] and can cleave both K63 and
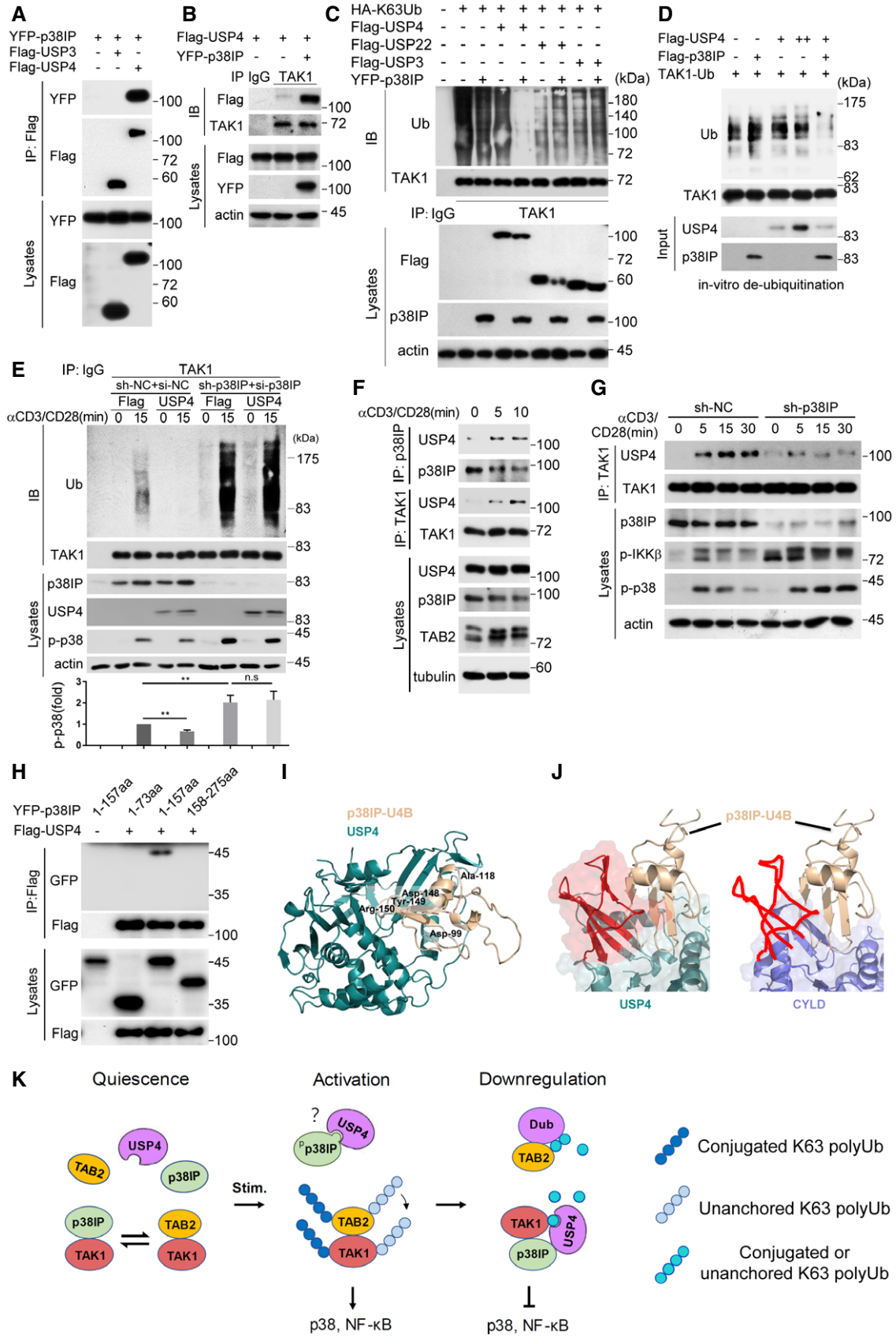
Figure 7.

◀

Figure 7. p38IP scaffolds USP4 to deubiquitinate TAK1.

A HEK293T cells co-transfected with YFP-p38IP and Flag vector, Flag-USP3 or Flag-USP4 as indicated were lysed and immunoprecipitated with anti-Flag antibody and immunoblotted with indicated antibodies.

B HEK293T cells transfected with Flag-USP4 and YFP vector or YFP-p38IP as indicated were lysed and immunoprecipitated with anti-IgG or anti-TAK1 and then immunoblotted with anti-Flag and anti-TAK1.

C HEK293T cells transfected with plasmids as indicated were lysed and immunoprecipitated with anti-TAK1, followed by *in vivo* ubiquitination assay of TAK1 as described in methods.

D *In vitro* deubiquitination assay of TAK1 as described in methods.

E sh-NC and sh-p38IP Jurkat E6.1 cells transfected with si-NC, si-p38IP, Flag, or Flag-USP4 as indicated were stimulated with anti-CD3/CD28 for 0 and 15 min at 48 h post-transfection, and then lysed and immunoprecipitated with anti-TAK1 under stringent conditions and immunoblotted with anti-ub. Statistical analysis of p-p38 levels was shown below the blot. **$P < 0.01$; n.s., not significant (two-tailed unpaired *t*-test, mean and s.e.m.).

F Jurkat E6.1 T cells were stimulated with anti-CD3/CD28 for the indicated times. The cell lysates were immunoprecipitated with anti-p38IP or anti-TAK1 and then immunoblotted with the indicated antibodies.

G sh-NC and sh-p38IP Jurkat E6.1 cells were stimulated with 10 μg/ml anti-CD3 plus 2 μg/ml anti-CD28 for the indicated times, and then lysed and immunoprecipitated with anti-TAK1 and immunoblotted with anti-USP4 and anti-TAK1.

H Mapping the USP4 binding domain of p38IP.

I Overall structure of p38IP U4B (gold) and USP4 (deep teal).

J Structural comparison between CYLD (blue) and USP4 (deep teal), the finger subdomain was shown in red.

K Schematic illustration of the molecular mechanism underlying p38IP regulation of TAK1. In quiescence state, p38IP constitutively competes with TABs for binding to TAK1. Upon receptor stimulation, p38IP transiently dissociates from TAK1 and increases its association with USP4, which might due to the phosphorylation of p38IP (indicated by an asterisk in the figure). Once TAK1 is activated, p38IP not only reassociates with TAK1, disassembling TABs-TAK1 complex and blocking the transfer of unanchored K63-linked polyUb chains from TAB2 to TAK1, but also specifically recruits USP4 to remove the unanchored K63-linked polyUb binding or conjugated ubiquitination of TAK1.

Data information: Data (A–H) are representatives of three independent experiments.
Source data are available online for this figure.

K48 linkages; therefore, p38IP-scaffolded USP4 probably exerts a function to cleave K48-K63 branched ubiquitin chains.

p38IP has been identified as human Spt20, which is a specific subunit of the human GCN5-SAGA complex that is highly similar to yeast Spt20 (ySpt20), containing a conserved Spt20 domain with unclear function [2,3]. In this study, we demonstrated that p38IP U4B (1–157 aa) functions to tether the deubiquitinase USP4, and since the Spt20 domain (74–226 aa) in p38IP overlaps with U4B, the Spt20 domain should function to tether DUBs. In fact, it has been reported that the deubiquitination activity of Ubp8, the homologue of human USP22 in *Saccharomyces cerevisiae*, toward H2B is dependent upon its association with the SAGA complex [67]. Additionally, the loss of ySpt20 protein increases H2B ubiquitination levels [68], suggesting that ySpt20 is required for the recruitment of Ubp8 to H2B. It has also been demonstrated that ySpt20 is required for the integrity of the SAGA complex [2,3], and p38IP maintains the stability of GCN5 and the integrity of the SAGA complex by inhibiting the ubiquitination of GCN5 [5]. Taken together, the above studies are in agreement with the present analysis, indicating that the Spt20 domain of p38IP is responsible for recruiting the deubiquitinase in both the TAK1 complex and the SAGA complex. Of note, there is no USP4 in yeast, suggesting that the p38IP-mediated TAK1-USP4 interaction only exists in mammalian cells. Notably, both GCN5 and USP22 are the bona fide components of the SAGA complex [57]; however, GCN5 could not be detected in TAK1 immunoprecipitates (Fig EV3C), and only USP4, but not USP22, deubiquitinated TAK1 in a p38IP-dependent manner (Figs 7E and EV5D), indicating that regulation of the TAK1 complex by p38IP in T cells may be SAGA-independent.

Our analysis of 60 randomly recruited patients diagnosed with RA showed a negative and significant correlation between the p38IP protein level in PBMCs and RA, suggesting a regulatory role for p38IP in the pathogenesis of RA. Coincidentally, a recent online study reported that a heterozygous non-sense SNV,

c.73T>A (p.Lys25*), located in the p38IP gene, which introduces a premature stop codon at the beginning of the gene (in the fourth exon), presented complete segregation with RA in an extended pedigree with early-onset cases [69]. The truncated p38IP (1–24 aa) resulting from this SNV lost almost all of the important domains, including the T1B domain and the main U4B domain (Fig EV5M), and thus could not inhibit immunoreceptor-induced TAK1 activation, which is essential for NF-κB and p38 activation. Therefore, the discoveries by us and Veyssiere *et al* could support each other and define an important role of p38IP in the pathogenesis of RA.

In summary, our findings revealed that p38IP is a negative regulator of TCR/LPS signaling pathways by competing with TABs for binding to TAK1 and scaffolding USP4 to ubiquitinated TAK1, indicating that p38IP functions as an intrinsic sensor of TAK1 activity to facilitate the accurate activation of TAK1. Moreover, p38IP may be involved in the regulation of inflammation and RA. This study delineates the unknown functions of p38IP and the underlying mechanism, revealing novel regulatory mechanisms for unanchored polyUb and TAK1 and providing new treatment strategies for autoimmune, inflammatory, and malignant diseases.

Materials and Methods

Antibodies and reagents

Anti-human CD3 (UCHT1) and anti-human CD28 (CD28.2) were from BD Pharmingen; anti-GCN5 (H-75; sc-20698), anti-IκB-α (C-21; sc-371), anti-p38IP (P-16; sc-84118), anti-p38IP (S-19; sc-84119), anti-β-actin (C4; sc-47778), anti-cMyc (9E10; sc-40), anti-YFP/GFP (B-2; sc-9996), anti-YFP/GFP (FL; sc-8334), anti-HA (F-7; sc-7392), anti-TRAF6 (H-274; sc-7221), anti-ub (P4D1; sc-8017), anti-TAK1

(M-17; sc-1839), anti-TAK1 (M-579; sc-7162), and anti-calnexin (AF18; sc-23954) were from Santa Cruz Biotechnology; anti-p-IκBα (ser32/36) (5A5; #9246), anti-p-p38 (Thr180/Tyr182) (12F8; #4631), anti-p-IKKα/β (Ser176/180) (16A6; #2697), anti-TAB1 (C25E9; #3226), anti-TAB2 (C88H10; #3744), and anti-K63 polyubiquitin (D7A11; #5621) were from CST; PE anti-human IL-2 and APC anti-human TNF-α were from eBioscience; anti-Flag (M2; F1804), PMA, ionomycin, LPS, and BFA were from Sigma-Aldrich; and lambda phosphatase were from New England Biolabs.

Human blood and RA samples

Human peripheral blood was obtained from healthy adult donors and donors with rheumatoid arthritis and provided by the General Hospital of Guangzhou Military Command of the PLA, and was handled under the guidelines of the Animal Care and Ethics committee of Sun Yat-Sen University. Sixty RA patients (the ratio of female to male is 4:1) who fulfilled the 1987 American College of Rheumatology (ACR) revised classification criteria for RA or the ACR/European League Against Rheumatism (EULAR) 2010 classification criteria for RA. The age range of the RA patients is 51–60 years old. Gender- and age-matched healthy volunteers ($n = 59$) were recruited as controls. Peripheral blood mononuclear cells (PBMCs) were isolated from peripheral blood using Ficoll (TBD Science) density gradient centrifugation. Total $CD4^+$ T cells were purified from PBMCs with anti-CD4 microbeads (Miltenyi Biotec) and cultured in RPMI-1640 medium (Corning Cellgro) supplemented with 10% (v/v) heat-inactivated FBS (Gibco), 2 mM glutamine.

Cell culture

HEK293T, THP-1, Jurkat E6.1, Jurkat Tag, and RAW264.7 cells (ATCC) were cultured in DMEM or RPMI1640 medium (Hyclone) supplemented with 10% FBS (Gibco) and 100 μg/ml penicillin and 100 U/ml streptomycin (Sigma). Mouse splenocytes were prepared from spleens of C57/B6 mice at 6–8 weeks old and were cultured in RPMI supplemented with 10% FBS.

Reporter gene assay

293T-MD2-TRL4 cells were transfected by Lipofectamine 2000 with NF-κB-, IFN-β-, or ISRE-luciferase reporter plasmids together with Flag-p38IP or Flag empty vectors. A control *Renilla* luciferase reporter vector was used for normalization. Twenty hours post-transfection, the cells were stimulated with or without 1 μg/ml LPS for 8 h, and luciferase activity in cell lysates was assayed for dual luciferase activity (Promega).

RNA-seq and data analysis

RNA-seq was performed by the Sequencing Platform BGISEQ-500 (BGI, Shenzhen, China). Briefly, sh-NC or sh-p38IP Jurkat E6.1 T cells were stimulated with anti-CD3 plus anti-CD28 for 3 h. Then, the total RNA of each sample was extracted, and a sequencing library was constructed. The differentially expressed genes (DEGs) were selected by using the threshold of fold change > 2 in expression between two treated groups (sh-p38IP vs. sh-NC, $P < 0.05$), and P value was calculated with Limma package (3.40.2) in R

(3.6.0). The transcript level was calculated according to the fragments per kilobase of transcript per million mapped reads (FPKM). Heatmap was conducted using the R package pheatmap. The selected 205 differentially expressed genes were subjected to Gene Ontology (GO), REACTOME Pathways (27.02.2019), and Kyoto Encyclopedia of Genes and Genomes (KEGG) analysis using ClueGo with the default parameters.

Real-time PCR

First Strand cDNA was synthesized by reverse transcription with oligo-dT and M-MLV reverse transcriptase (Promega) from total RNA extracted from various cells using TRIzol reagent (Invitrogen). Real-time fluorescence-based quantitative PCR was run on a Light-Cycler 480 system (Roche) with the SYBR Green I Master (Roche). PCR was performed by denaturing at 95°C for 5 min, followed by 40 cycles of denaturation at 95°C, annealing at 60°C, and extension at 72°C for 20 s. Results were normalized with GADPH. For primer sequences, see Appendix Table S1.

Immunoprecipitation and immunoblot analysis

For immunoprecipitation, cells were lysed with lysis buffer (1% NP-40, 5 mM NaPPi, 150 mM NaCl, 20 mM Tris–HCl, pH 7.5, 5 mM EDTA, 1 mM Na_3VO_4, 1 mM PMSF, 100 μg/ml Aprotinin, 10 μg/ml Leupeptin) after transfection or stimulation with indicated ligands, and cell lysates were clarified by centrifugation followed by incubation overnight with the indicated antibodies and then incubated with protein G beads (GE Healthcare) for additional 4 h. Beads were then washed for at least three times with lysis buffer, and proteins were eluted with 2× SDS Loading Buffer and resolved by SDS–PAGE, transferred onto a PVDF membrane and visualized using secondary antibodies conjugated to avidin–horseradish peroxidase with ECL reagent.

In vitro kinase assay

For TAK1 kinase assay, the cell lysates of resting or stimulated cells were immunoprecipitated with anti-TAK1 and protein G beads. The beads were washed three times with lysis buffer and two times with kinase buffer (25 mM Tris at pH 7.5, 2 mM DTT, 0.1 mM Na_3VO_4, 10 mM $MgCl_2$). Immunoprecipitates were resuspended in kinase buffer containing 100 μM ATP and 1 μg recombinant GST-IKKβ (111–250 aa) protein purified *Escherichia coli* as substrate for TAK1, then the mixture was incubated at 30°C with gently shaking for 30 min, and the reaction was terminated by addition of SDS loading Buffer and resolved by SDS–PAGE.

ELISA and intracellular cytokine staining

Human IL-2, IL-6, and TNF-α, and mouse IL-1β, IL-6, and IFN-β were detected with ELISA kits according to the manufactory's protocol (eBiosciecne), and mouse IFN-β ELISA kit was from BioLegend. For intracellular cytokine staining, cells were stimulated with appropriate ligands along with 10 μg/ml BFA (Sigma) for 6 h at 37°C, then washed once with PBS, resuspended in 250 μl Cytofix/Cytoperm buffer (BD Pharmingen), and incubated for 20 min at 4°C. Then, the cells were washed twice with 1 ml Perm/Wash buffer

(1% BSA/0.5% Saponin/PBS) and resuspended in 100 μl of Perm/ Wash buffer containing appropriate fluorophore-conjugated anti- bodies. After incubation at 4°C in darkness for 30 min, cells were washed three times with Perm/Wash buffer, resuspended in 300 μl PBS/BSA, and analyzed with FACSCalibur (BD).

Mass spectrometry

Jurkat TAg cells were harvested and lysed. After clearance by centrifugation, whole-cell lysates were incubated overnight with the TAK1 antibody, and proteins were immunoprecipitated for an addi- tional 4 h at 4 °C with protein G-Sepharose beads (GE Healthcare). Immunoprecipitates were extensively washed five times with lysis buffer and were separated by SDS–PAGE. Then, the gel panel containing 70–140 kDa bands was excised from the Coomassie blue-stained gel and analyzed by liquid chromatography–tandem MS. The proteins were reduced, alkylated, and digested with trypsin in-gel as described [70]. After the desalting procedure, the peptides were analyzed by the LTQ Orbitrap Elite system and Easy-nLC 1000 system (Thermo Fisher Scientific).

In vivo K63-polyUb binding and ubiquitination assay

Cells were transfected or treated as indicated and then lysed in lysis buffer (1% NP-40) containing 20 mM N-ethylmaleimide. After cell lysates were clarified by centrifugation, for K63-polyUb binding assay, target proteins were immunoprecipitated and blotted with anti-K63 polyUb; for ubiquitination assay, 1% SDS (v/v) was added to the supernatants and proteins were dissociated by heating at 90°C for 10 min, and samples were diluted 1:10 with lysis buffer. Endogenous or transfected protein was immunoprecipitated with indicated antibodies and protein G beads. Immunoprecipitates were washed four times with lysis buffer and prepared for immunoblot analysis as indicated.

In vitro polyUb binding assay

GST-fused proteins were expressed in *E. coli* and purified from bacterial lysates by binding to glutathione-Sepharose beads. K63- linked polyubiquitin chains (ub_2-ub_7) were purchased from Boston Biochem. Recombinant full-length or truncated GST-TAK1 proteins (about 5 μg each) immobilized on glutathione-Sepharose beads were incubated, respectively, with 0.5 μg K63-linked polyUb chains in binding buffer (25 mM HEPES at pH 7.4, 150 mM KCl, 2 mM $MgCl_2$, 0.5% Triton X-100, 1 mM EGTA, and 1 mg/ml BSA) for 2 h at 4°C, followed by washing with the ubiquitin binding buffer and boiled in SDS loading buffer.

In vitro deubiquitination assay

HEK293T cells were transfected with Flag-USP4 and Flag-p38IP and lysed with lysis buffer 24 h later, and USP4 and p38IP were immunoprecipitated with anti-Flag followed by elution with 15 mg/ ml Flag peptide. Ubiquitinated TAK1 was immunoprecipitated from lysates of Jurkat E6.1 cells stimulated with anti-CD3 and anti-CD28 for 5 min in lysis buffer containing 1% SDS. The purified ubiquiti- nated TAK1 precipitates were incubated with purified Flag-USP4 or Flag-p38IP proteins as indicated in the deubiquitination buffer [71]

(50 mM Tris–HCl, pH 8.0; 50 mM NaCl; 1 mM EDTA; 10 mM DTT, and 5% glycerol) at 37°C for 2 h. TAK1 ubiquitination was detected by immunoblotting with anti-ub antibodies.

3D structure modeling and docking analysis

The 3D structure of p38IP T1B and U4B domains were predicted using i-tasser [72] and Phyre2 protein fold recognition server [60], respectively. To evaluate the quality of the predicted structure, assessment tools such as Ramachandran plot and VERIFY3D [73] were used and the best-ranked model was selected for further docking analysis. Protein–protein docking was performed with PIPER, Maestro (Schrödinger Release 2018-1: Schrödinger, LLC, New York, NY, 2018) in the mode of receptor–ligand interaction. In brief, the crystal structure of Dusp-Ubl and D1D2 domains of Usp4 (PDB: 5CTR and 2Y6E) were set as receptors, and the predicted structure of p38IP U4B was set as a ligand. All the mole- cules were prepared using two steps in "protein preparation wizard" (default parameters) in Maestro interface and refined for docking analysis, which added hydrogens to the model proteins, and optimized the charged states of amino acids. The restrained amino acids were defined to the three conserved loops of p38IP- U4B. Based on the computed docking rank, the best pose was chosen for further analysis. The T1B-TAK1 docking model was generated using a similar strategy.

Statistical analysis

Statistical significance was quantified by *P*-values using GraphPad Prism v5.0 software. Two-tailed Student's *t*-test was used for compar- isons between two groups. For all tests, differences were considered statistically significant when *P*-values were below 0.05 (*), 0.01 (**), 0.001 (***), or 0.0001 (****). In the figures, *P*-values are indicated as follows: *P < 0.05; **P < 0.01; ***P < 0.001; ****P < 0.0001 and ns, not significant. Graphs represent mean ± standard error of the mean (s.e.m.).

Data availability

RNA-seq data reported in this study have been deposited with the Sequence Read Archive under the accession BioProject ID PRJNA622664 (https://www.ncbi.nlm.nih.gov/Traces/study/?acc = PRJNA622664). Mass spectrometry proteomic data from this study have been deposited to the ProteomeXchange-PRIDE repository (https://www.ebi.ac.uk/pride/archive/) and assigned the dataset number PXD018330.

Expanded View for this article is available online.

Author contributions

Conflict of interest

References

1. Zohn IE, Li Y, Skolnik EY, Anderson KV, Han J, Niswander L (2006) p38 and a p38-interacting protein are critical for downregulation of E-cadherin during mouse gastrulation. *Cell* 125: 957–969

2. Wang YL, Faiola F, Xu M, Pan S, Martinez E (2008) Human ATAC is a GCN5/PCAF-containing acetylase complex with a novel NC2-like histone fold module that interacts with the TATA-binding protein. *J Biol Chem* 283: 33808–33815

3. Nagy Z, Riss A, Romier C, le Guezennec X, Dongre AR, Orpinell M, Han J, Stunnenberg H, Tora L (2009) The human SPT20-containing SAGA complex plays a direct role in the regulation of endoplasmic reticulum stress-induced genes. *Mol Cell Biol* 29: 1649–1660

4. Webber JL, Tooze SA (2010) Coordinated regulation of autophagy by p38alpha MAPK through mAtg9 and p38IP. *EMBO J* 29: 27–40

5. Liu X, Xiao W, Wang XD, Li YF, Han J, Li Y (2013) The p38-interacting protein (p38IP) regulates G2/M progression by promoting alpha-tubulin acetylation via inhibiting ubiquitination-induced degradation of the acetyltransferase GCN5. *J Biol Chem* 288: 36648–36661

6. Yu X, Wang QL, Li YF, Wang XD, Xu A, Li Y (2016) A novel miR-200b-3p/p38IP pair regulates monocyte/macrophage differentiation. *Cell Discov* 2: 15043

7. Liu T, Zhang L, Joo D, Sun SC (2017) NF-kappaB signaling in inflammation. *Signal Transduct Target Ther* 2: 17023

8. Zarubin T, Han J (2005) Activation and signaling of the p38 MAP kinase pathway. *Cell Res* 15: 11–18

9. Shim JH, Xiao C, Paschal AE, Bailey ST, Rao P, Hayden MS, Lee KY, Bussey C, Steckel M, Tanaka N *et al* (2005) TAK1, but not TAB1 or TAB2, plays an essential role in multiple signaling pathways *in vivo*. *Genes Dev* 19: 2668–2681

10. Sato S, Sanjo H, Takeda K, Ninomiya-Tsuji J, Yamamoto M, Kawai T, Matsumoto K, Takeuchi O, Akira S (2005) Essential function for the kinase TAK1 in innate and adaptive immune responses. *Nat Immunol* 6: 1087–1095

11. Wan YY, Chi H, Xie M, Schneider MD, Flavell RA (2006) The kinase TAK1 integrates antigen and cytokine receptor signaling for T cell development, survival and function. *Nat Immunol* 7: 851–858

12. Shibuya H, Yamaguchi K, Shirakabe K, Tonegawa A, Gotoh Y, Ueno N, Irie K, Nishida E, Matsumoto K (1996) TAB1: an activator of the TAK1 MAPKKK in TGF-beta signal transduction. *Science* 272: 1179–1182

13. Takaesu G, Kishida S, Hiyama A, Yamaguchi K, Shibuya H, Irie K, Ninomiya-Tsuji J, Matsumoto K (2000) TAB2, a novel adaptor protein, mediates activation of TAK1 MAPKKK by linking TAK1 to TRAF6 in the IL-1 signal transduction pathway. *Mol Cell* 5: 649–658

14. Cheung PC, Nebreda AR, Cohen P (2004) TAB3, a new binding partner of the protein kinase TAK1. *Biochem J* 378: 27–34

15. Ishitani T, Takaesu G, Ninomiya-Tsuji J, Shibuya H, Gaynor RB, Matsumoto K (2003) Role of the TAB2-related protein TAB3 in IL-1 and TNF signaling. *EMBO J* 22: 6277–6288

16. Kishimoto K, Matsumoto K, Ninomiya-Tsuji J (2000) TAK1 mitogen-activated protein kinase kinase kinase is activated by autophosphorylation within its activation loop. *J Biol Chem* 275: 7359–7364

17. Besse A, Lamothe B, Campos AD, Webster WK, Maddineni U, Lin SC, Wu H, Darnay BG (2007) TAK1-dependent signaling requires functional interaction with TAB2/TAB3. *J Biol Chem* 282: 3918–3928

18. Kulathu Y, Akutsu M, Bremm A, Hofmann K, Komander D (2009) Two-sided ubiquitin binding explains specificity of the TAB2 NZF domain. *Nat Struct Mol Biol* 16: 1328

19. Sato Y, Yoshikawa A, Yamashita M, Yamagata A, Fukai S (2009) Structural basis for specific recognition of Lys 63-linked polyubiquitin chains by NZF domains of TAB2 and TAB3. *EMBO J* 28: 3903–3909

20. Chen ZJ (2012) Ubiquitination in signaling to and activation of IKK. *Immunol Rev* 246: 95–106

21. Hirata Y, Takahashi M, Morishita T, Noguchi T, Matsuzawa A (2017) Post-translational modifications of the TAK1-TAB complex. *Int J Mol Sci* 18: E205

22. Hu H, Sun SC (2016) Ubiquitin signaling in immune responses. *Cell Res* 26: 457–483

23. Kanayama A, Seth RB, Sun L, Ea CK, Hong M, Shaito A, Chiu YH, Deng L, Chen ZJ (2004) TAB2 and TAB3 activate the NF-kappaB pathway through binding to polyubiquitin chains. *Mol Cell* 15: 535–548

24. Strickson S, Emmerich CH, Goh ETH, Zhang J, Kelsall IR, Macartney T, Hastie CJ, Knebel A, Peggie M, Marchesi F *et al* (2017) Roles of the TRAF6 and Pellino E3 ligases in MyD88 and RANKL signaling. *Proc Natl Acad Sci USA* 114: E3481–E3489

25. Xia ZP, Sun L, Chen X, Pineda G, Jiang X, Adhikari A, Zeng W, Chen ZJ (2009) Direct activation of protein kinases by unanchored polyubiquitin chains. *Nature* 461: 114–119

26. Pertel T, Hausmann S, Morger D, Zuger S, Guerra J, Lascano J, Reinhard C, Santoni FA, Uchil PD, Chatel L *et al* (2011) TRIM5 is an innate immune sensor for the retrovirus capsid lattice. *Nature* 472: 361–365

27. Gaud G, Lesourne R, Love PE (2018) Regulatory mechanisms in T cell receptor signalling. *Nat Rev Immunol* 18: 485–497

28. Liu J, Cao X (2016) Cellular and molecular regulation of innate inflammatory responses. *Cell Mol Immunol* 13: 711–721

29. Angelotti F, Parma A, Cafaro G, Capecchi R, Alunno A, Puxeddu I (2017) One year in review 2017: pathogenesis of rheumatoid arthritis. *Clin Exp Rheumatol* 35: 368–378

30. Calabresi E, Petrelli F, Bonifacio AF, Puxeddu I, Alunno A (2018) One year in review 2018: pathogenesis of rheumatoid arthritis. *Clin Exp Rheumatol* 36: 175–184

31. Malemud CJ (2018) Defective T-cell apoptosis and T-regulatory cell dysfunction in rheumatoid arthritis. *Cells* 7: E223

32. Han J, Ulevitch RJ (2005) Limiting inflammatory responses during activation of innate immunity. *Nat Immunol* 6: 1198–1205

33. Yamamoto M, Sato S, Hemmi H, Hoshino K, Kaisho T, Sanjo H, Takeuchi O, Sugiyama M, Okabe M, Takeda K *et al* (2003) Role of adaptor TRIF in the MyD88-independent toll-like receptor signaling pathway. *Science* 301: 640–643

34. Faure E, Equils O, Sieling PA, Thomas L, Zhang FX, Kirschning CJ, Polentarutti N, Muzio M, Arditi M (2000) Bacterial lipopolysaccharide activates NF-kappaB through toll-like receptor 4 (TLR-4) in cultured human dermal endothelial cells. Differential expression of TLR-4 and TLR-2 in endothelial cells. *J Biol Chem* 275: 11058–11063

35. McInnes IB, Schett G (2007) Cytokines in the pathogenesis of rheumatoid arthritis. *Nat Rev Immunol* 7: 429–442

36. Schieven GL (2009) The p38alpha kinase plays a central role in inflammation. *Curr Top Med Chem* 9: 1038–1048

37. Thalhamer T, McGrath MA, Harnett MM (2008) MAPKs and their relevance to arthritis and inflammation. *Rheumatology (Oxford)* 47: 409–414

38. Brown KD, Claudio E, Siebenlist U (2008) The roles of the classical and alternative nuclear factor-kappaB pathways: potential implications for autoimmunity and rheumatoid arthritis. *Arthritis Res Ther* 10: 212

39. Simmonds RE, Foxwell BM (2008) Signalling, inflammation and arthritis: NF-kappaB and its relevance to arthritis and inflammation. *Rheumatology (Oxford)* 47: 584–590

40. Li Q, Verma IM (2002) NF-kappaB regulation in the immune system. *Nat Rev Immunol* 2: 725–734

41. Ashwell JD (2006) The many paths to p38 mitogen-activated protein kinase activation in the immune system. *Nat Rev Immunol* 6: 532–540

42. Fitzgerald KA, McWhirter SM, Faia KL, Rowe DC, Latz E, Golenbock DT, Coyle AJ, Liao SM, Maniatis T (2003) IKKepsilon and TBK1 are essential components of the IRF3 signaling pathway. *Nat Immunol* 4: 491–496

43. Cheung PC, Campbell DG, Nebreda AR, Cohen P (2003) Feedback control of the protein kinase TAK1 by SAPK2a/p38alpha. *EMBO J* 22: 5793–5805

44. Liu HH, Xie M, Schneider MD, Chen ZJ (2006) Essential role of TAK1 in thymocyte development and activation. *Proc Natl Acad Sci USA* 103: 11677–11682

45. Sun L, Deng L, Ea CK, Xia ZP, Chen ZJ (2004) The TRAF6 ubiquitin ligase and TAK1 kinase mediate IKK activation by BCL10 and MALT1 in T lymphocytes. *Mol Cell* 14: 289–301

46. Jiang Z, Mak TW, Sen G, Li X (2004) Toll-like receptor 3-mediated activation of NF-kappaB and IRF3 diverges at Toll-IL-1 receptor domain-containing adapter inducing IFN-beta. *Proc Natl Acad Sci USA* 101: 3533–3538

47. Wang C, Deng L, Hong M, Akkaraju GR, Inoue J, Chen ZJ (2001) TAK1 is a ubiquitin-dependent kinase of MKK and IKK. *Nature* 412: 346–351

48. Salvador JM, Mittelstadt PR, Guszczynski T, Copeland TD, Yamaguchi H, Appella E, Fornace AJ Jr, Ashwell JD (2005) Alternative p38 activation pathway mediated by T cell receptor-proximal tyrosine kinases. *Nat Immunol* 6: 390–395

49. Wu CJ, Conze DB, Li T, Srinivasula SM, Ashwell JD (2006) Sensing of Lys 63-linked polyubiquitination by NEMO is a key event in NF-kappaB activation [corrected]. *Nat Cell Biol* 8: 398–406

50. Husnjak K, Dikic I (2012) Ubiquitin-binding proteins: decoders of ubiquitin-mediated cellular functions. *Annu Rev Biochem* 81: 291–322

51. Totzke J, Gurbani D, Raphemot R, Hughes PF, Bodoor K, Carlson DA, Loiselle DR, Bera AK, Eibschutz LS, Perkins MM *et al* (2017) Takinib, a selective TAK1 inhibitor, broadens the therapeutic efficacy of TNF-alpha inhibition for cancer and autoimmune disease. *Cell Chem Biol* 24: 1029–1039 e7

52. Reiley WW, Jin W, Lee AJ, Wright A, Wu X, Tewalt EF, Leonard TO, Norbury CC, Fitzpatrick L, Zhang M *et al* (2007) Deubiquitinating enzyme CYLD negatively regulates the ubiquitin-dependent kinase Tak1 and prevents abnormal T cell responses. *J Exp Med* 204: 1475–1485

53. Ahmed N, Zeng M, Sinha I, Polin L, Wei WZ, Rathinam C, Flavell R, Massoumi R, Venuprasad K (2011) The E3 ligase Itch and deubiquitinase Cyld act together to regulate Tak1 and inflammation. *Nat Immunol* 12: 1176–1183

54. Fan YH, Yu Y, Mao RF, Tan XJ, Xu GF, Zhang H, Lu XB, Fu SB, Yang J (2011) USP4 targets TAK1 to downregulate TNFalpha-induced NF-kappaB activation. *Cell Death Differ* 18: 1547–1560

55. Liang L, Fan Y, Cheng J, Cheng D, Zhao Y, Cao B, Ma L, An L, Jia W, Su X *et al* (2013) TAK1 ubiquitination regulates doxorubicin-induced NF-kappaB activation. *Cell Signal* 25: 247–254

56. Yang Z, Xian H, Hu J, Tian S, Qin Y, Wang RF, Cui J (2015) USP18 negatively regulates NF-kappaB signaling by targeting TAK1 and NEMO for deubiquitination through distinct mechanisms. *Sci Rep* 5: 12738

57. Zhang XY, Varthi M, Sykes SM, Phillips C, Warzecha C, Zhu W, Wyce A, Thorne AW, Berger SL, McMahon SB (2008) The putative cancer stem cell marker USP22 is a subunit of the human SAGA complex required for activated transcription and cell-cycle progression. *Mol Cell* 29: 102–111

58. Cui J, Song Y, Li Y, Zhu Q, Tan P, Qin Y, Wang HY, Wang RF (2014) USP3 inhibits type I interferon signaling by deubiquitinating RIG-I-like receptors. *Cell Res* 24: 400–416

59. Soukenik M, Diehl A, Leidert M, Sievert V, Bussow K, Leitner D, Labudde D, Ball LJ, Lechner A, Nagler DK *et al* (2004) The SEP domain of p47 acts as a reversible competitive inhibitor of cathepsin L. *FEBS Lett* 576: 358–362

60. Kelley LA, Mezulis S, Yates CM, Wass MN, Sternberg MJ (2015) The Phyre2 web portal for protein modeling, prediction and analysis. *Nat Protoc* 10: 845–858

61. Sato Y, Goto E, Shibata Y, Kubota Y, Yamagata A, Goto-Ito S, Kubota K, Inoue J, Takekawa M, Tokunaga F *et al* (2015) Structures of CYLD USP with Met1- or Lys63-linked diubiquitin reveal mechanisms for dual specificity. *Nat Struct Mol Biol* 22: 222–229

62. Selimkhanov J, Taylor B, Yao J, Pilko A, Albeck J, Hoffmann A, Tsimring L, Wollman R (2014) Systems biology. Accurate information transmission through dynamic biochemical signaling networks. *Science* 346: 1370–1373

63. Cohen P (2018) Ubiquitin chains as second messengers. *Nat Rev Mol Cell Biol* 19: 212

64. Wertz IE, Dixit VM (2010) Signaling to NF-kappaB: regulation by ubiquitination. *Cold Spring Harb Perspect Biol* 2: a003350

65. Ohtake F, Saeki Y, Ishido S, Kanno J, Tanaka K (2016) The K48-K63 branched ubiquitin chain regulates NF-kappaB signaling. *Mol Cell* 64: 251–266

66. Ye Y, Scheel H, Hofmann K, Komander D (2009) Dissection of USP catalytic domains reveals five common insertion points. *Mol BioSyst* 5: 1797–1808

67. Lee KK, Florens L, Swanson SK, Washburn MP, Workman JL (2005) The deubiquitylation activity of Ubp8 is dependent upon Sgf11 and its association with the SAGA complex. *Mol Cell Biol* 25: 1173–1182

68. Henry KW, Wyce A, Lo WS, Duggan LJ, Emre NC, Kao CF, Pillus L, Shilatifard A, Osley MA, Berger SL (2003) Transcriptional activation via sequential histone H2B ubiquitylation and deubiquitylation, mediated by SAGA-associated Ubp8. *Genes Dev* 17: 2648–2663

69. Veyssiere M, Perea J, Michou L, Boland A, Caloustian C, Olaso R, Deleuze J-F, Cornelis F, Petit-Teixeira E, Chaudru V (2019) A novel nonsense variant in SUPT20H gene associated with rheumatoid arthritis identified by whole exome sequencing of multiplex families. *PLoS ONE* 14: e0213387

70. Wang XD, Gong Y, Chen ZL, Gong BN, Xie JJ, Zhong CQ, Wang QL, Diao LH, Xu A, Han J *et al* (2015) TCR-induced sumoylation of the kinase PKC-theta controls T cell synapse organization and T cell activation. *Nat Immunol* 16: 1195–1203

71. Lin Z, Yang H, Kong Q, Li J, Lee SM, Gao B, Dong H, Wei J, Song J, Zhang DD *et al* (2012) USP22 antagonizes p53 transcriptional activation by deubiquitinating Sirt1 to suppress cell apoptosis and is required for mouse embryonic development. *Mol Cell* 46: 484−494

72. Yang J, Yan R, Roy A, Xu D, Poisson J, Zhang Y (2015) The I-TASSER Suite: protein structure and function prediction. *Nat Methods* 12: 7−8

73. Luthy R, Bowie JU, Eisenberg D (1992) Assessment of protein models with three-dimensional profiles. *Nature* 356: 83−85